IMECHE J. NANOMATERIALS, NANOENGINEERING AND NANOSYSTEMS (UK)

https://journals.sagepub.com/home/pin

ACCEPTED 26 JANUARY 2024

TRIPLE DIFFUSIVE FREE MAGNETO-CONVECTION OF ELECTRO-CONDUCTIVE NANOFLUID FROM A VERTICAL STRETCHING SHEET

B. Vasu[1]*, O. Anwar Bég[2], Mustaque Hussain Borbora[1], Rama Subba Reddy Gorla[3],

Jayati Tripathi[1] and M.L. Burby[2]

[1]Department of Mathematics, Motilal Nehru National Institute of Technology Allahabad, Prayagraj, Uttar Pradesh- 211004, ***India***
[2]Professor and Director-MPESG, Corrosion Lab, 3-08, Department of Mechanical and Aeronautical Engineering, SEE Bldg, Salford University, Manchester, M54WT, ***UK****.*
[3]Department of Aeronautics and Astronautics, Air Force Institute of Technology, Wright Patterson Air Force Base, Dayton, Ohio 45433, ***USA***
**Corresponding author- email:* bvasu@mnnit.ac.in

Abstract:

In the present investigation, an analysis is carried out to study the MHD triple diffusive free thermo-solutal convection boundary layer flow of an electro-conductive nanofluid flow over a vertical porous stretching sheet. This problem is relevant to magnetic nanomaterials fabrication operations in which multiple species in addition to nanoparticles are present. In addition to the nanoparticle diffusion, two different salts (species) having different properties are considered. A variable magnetic field is applied transverse to the vertical sheet. It is assumed that the surface is in contact with the hot magnetic nanofluid at a temperature which provides a variable heat transfer coefficient. Buongiorno model is employed for the nanofluid. It is also assumed that the Oberbeck-Boussinesq approximation is valid and the mixture of nanofluid and salts is homogenous and is in local thermal equilibrium. In addition, the thermal energy equation features cross-diffusion (Soret and Dufour) terms for both components of salts having different concentration. Appropriate similarity transformations are deployed to render the model non-dimensional. The emerging transformed dimensionless non-linear non-dimensional ordinary differential boundary value problem is solved with the robust bvp4c method in MATLAB. The simulations show that the addition of nanoparticles and salts, strongly modifies teperature and nanoparticle and salt 1 and 2 concentrations. With stronger magnetic field the velocity is suppressed as is momentum boundary layer thickness whereas temperatures are boosted.

Keywords: *Triple diffusive convection; Magnetic nanofluids; Stretching sheet; Dufour and Soret effects; Boussinesq approximation; Salts; Lewis number; suction/injection; coating flow.*

1 Introduction:

Conventional heat transfer fluids such as water, ethylene glycol mixture and engine oil have limited heat transfer capabilities due to their low thermal conductivity in enhancing the performance and compactness of many engineering electronic devices. In contrast, metals have thermal conductivities up to three times higher than these fluids. Thus, it is naturally desirable to combine the two substances to produce a medium for heat transfer that would behave like a fluid but has the enhanced thermal conductivity benefits of a metal. Therefore, there is a strong need to develop advanced heat transfer fluids with substantially higher conductivities to enhance thermal characteristics. The terminology of *nanofluid* (nanoparticle fluid suspension) was introduced by Choi [1] to describe this new class of nanotechnology-based heat transfer fluids that exhibit thermal properties superior to those of their host (based) fluids. Modern nanotechnology can produce metallic or non-metallic particles with average sizes below 100nm in traditional heat transfer (base) fluids such as water, oil, and ethylene glycol [2,3]. Nanofluids may be used in various applications which include coating [4], solar panels [5], thermally efficient coolants for nuclear reactors [6], heat exchangers [7], tribology [8], PEM fuel cells [9], sterilization in biomedicine [10], nano-drug delivery in pharmacology [11], hybrid direct absorption solar collectors [12], materials processing [13], electronic cooling, transformers, rocket fuels etc Nanofluids technology, a new interdisciplinary field of growing importance combines nanoscience, nanotechnology and thermal engineering and has expanded significantly over the past two decades. As it is already well known, the main scope of nanofluids is the enhancement of thermal conductivity of liquids, which is an extremely important topic from the energy efficiency point of view. Choi *et al.* [3] showed that the addition of small amount (less than 1% by volume) of nanoparticles to conventional heat transfer liquids can successfully enhance the thermal conductivity of the fluid up to approximately two times. They also noted that above volume fractions of 8% this trend can be reversed due to agglomeration effects, so that there is a critical range of nanoparticle doping which produces benefits.

The analysis of the flow field in the boundary-layer near a stretching sheet is a of considerable relevance to a number of engineering processes such as extrusion of plastic sheets, polymer processing, coating deposition and thin film nanomaterials fabrication [14]. Both carbon-based (e. g. SiC, graphene etc) and metallic nanoparticles (e.g. Tantalum, zinc, magnesium oxide etc) have been explored in these applications. A popular approach for theoretical simulation of nanofluid flows is the Buongiorno two-component nanoscale model which features

conservation equations for both heat transport and nanoparticle diffusion. This approach comfortably accommodates boundary layer flows and has been adopted extensively in recent years. Two prominent features of the Buongiorno model are thermophoresis and Brownian dynamics. While specific nanomaterial particle types cannot be assessed with this model, it does provide a good insight into the thermo-solutal transport characteristics. Early applications of the Buongiorno model considered free convection nanofluid boundary layers from vertical stationary surfaces [16, 17]. Khan and Pop [18] generalized these studies to consider stretching boundaries. More recently Ray *et al*. [19] further extended these works to address non-Fourier (thermal relaxation effects) in nanofluid polymer boundary layer flows and also considered non-Newtonian effects. Further investigations of *external boundary layer convection flows* of nanofluids using the Buongiorno model have been communicated by Ray *et al*. [20] (for wedge and cone geometries) and Vasu *et al.* [21] (who also addressed second law thermodynamics an inclined boundary effects).

More recently a new sub-branch of nanofluids has emerged. Magnetic nanofluids are synthesized by deploying magnetic nanoparticles in base liquids such as polymers. The resulting suspension exhibits electro-conductive properties which can be manipulated via external magnetic fields. Magnetic nanofluids therefore combine the thermal enhancement properties of standard unitary or hybrid nanofluids with smart electromagnetic properties [22]. This dual capability has witnessed the deployment of magnetic nanofluids in a wide spectrum of applications including substrate coating [23], smart pumping systems for bio-microfluidics [24], ferromagnetic spin coating [25], additive manufacturing of conducting nano-polymers [26, 27] and next generation functional sensor nano-magnetic coatings [28] To simulate magnetic nanofluid flows the equations of magnetohydrodynamics (MHD) must be combined with nanofluid mechanics. Stretching sheet flows of magnetic nanofluids have been addressed by several investigators. Anwar *et al.* [29] considered exponential stretching velocity, magnetic induction and viscoelastic effects. They showed that temperature and concentration are reduced with greater viscoelastic effect and Nusselt number is reduced with magnetic body force parameter and magnetic Prandtl number. They also found that Nusselt number is boosted with Brownian motion and thermophoresis effects whereas Sherwood number is reduced with thermophoresis. Further studies using the Buongiorno nanoscale model include Hussain et al. [30] (who included radiative flux effects) and Bég *et al.* [31] (who additionally addressed time-dependent and porous media effects).

In the manipulation of polymer material characteristics [14], it is important to include thermo-diffusion and diffuso-thermal effects which respectively consider the influence of *concentration gradients on the temperature field* and the impact of *temperature gradients on the concentration field*. These collective diffusive phenomena become prominent when density differences exist in the flow regime and are frequently termed *cross-diffusion* effects in heat and mass transfer analysis. With judicious selection of different species e. g. salts embedded in nano-polymers, the structure of the polymer can be modified and customized for specific bespoke applications [32] which enhances product quality and consistency. Effectively when heat and mass transfer occurred in a moving fluid, the energy flux can be generated by a composition gradient, namely, the Dufour or diffusion- thermo effect, and the mass fluxes developed by the temperature gradients via the Soret or thermal-diffusion effect. In the mathematical modelling community, therefore, substantial interest has emerged in studying Soret and Dufour effects in both conventional polymeric flows and nano-polymers. Hayat and Hendi [33] used a homotopy analysis method to compute the Soret-Dufour effects in Hall magneto-convective viscolastic flow from an extending surface. Afify [34] investigated the magnetohydrodynamic thermo-solutal convection from a linear stretching surface with wall mass flux and Soret-Dufour effects. He showed for fluent media with medium molecular weight (H_2, air), Dufour and Soret effects become significant, and that greater wall suction suppresses the momentum boundary layer thickness. Das *et al.* [35] considered heat and mass transfer in free convective hyromagnetic flow past a vertical porous plate, observing that greater Soret number enhances concentration magnitudes whereas increasing Schmidt number suppresses Sherwood number (wall mass transfer rate). Bég *et al.* [36] used a finite difference technique to compute the Soret-Dufour effects in micropolar boundary layer flow from a spherical body. They noted that mass transfer to the sphere surface is depleted with both increment in Soret and Dufour numbers i. e. Sherwood number is reduced. However, Nusselt number was shown to be elevated with greater Soret number and suppressed with larger Dufour number. More recently cross diffusion effects in nanofluid boundary layer flows have been examined. Relevant studies include Dzulkifli *et al.* [37] (who considered unsteady stretching/contracting sheet flow) and Umavathi and Bég [38] (who simulated hybrid carbon/metallic nanofluids in vertical duct flows). Soret and Dufour effects in magnetic nanofluids have been investigated by Anwar *et al.* [39]. They considered a stretching sheet in thermally stratified nanofluid media under a transverse magnetic field and showed that temperatures are boosted with Brownian and thermophoretic parameters whereas they are depleted with Dufour number. Increasing Soret number was also found to significantly increase

nanoparticle concentration boundary layer thickness. Bhatti *et al*. [40] investigated the ferric oxide (Fe3O4-water) magnetic nanofluid flow from a nonlinear stretching porous sheet in porous media with Soret-Dufour, slip and radiative heat transfer effects. They found that thermal boundary layer thickness is increased with Dufour number and radiative parameter whereas nanoparticle concentration magnitudes are elevated with Soret number.

The above studies considered only single species (nanoparticle) diffusion in magnetic nanofluid transport. However, in triple diffusion, two separate species are present [41]. Umavathi and Bég [42] conducted a perturbation study of triple diffusion in a vertical duct with mixed derivative convective wall heating conditions and dissipation effects. They utilized two solutal Grashof numbers (one for each of the diffusing components, i.e., species 1 and species 2) and noted that increment in the second species (salt) solutal Grashof number retards the flow in the left duct half space whereas it accelerates the flow in the right duct half space but suppresses temperatures across the entire duct width. Frequently salts are also deployed to modify the constitution of nanofluid media including magnetic nano-polymers [28]. The simulation of these supplementary diffusive phenomena requires additional conservation equations for the additional diffusing species (salts) in addition to the Buongiorno formulation for heat and nanoparticle diffusion. Khan *et al.* [43] have presented one of the few studies of triple convective diffusion in nanofluid boundary layer along a vertical surface in porous media. They demonstrated that Nusselt number is strongly enhanced with the combined mass flux effects of nanoparticles and salts.

An inspection of the literature has revealed that previous studies did not consider *magnetic nanofluids with triple diffusion from a vertical stretching sheet*. This is the novelty of the current study. Motivated by emerging applications in smart electromagnetic nano-polymers [28, 29, 44], which combine the deployment of dual species (salts) and magnetic nanoparticles to modify thermo/solutal characteristics, in the present article, a mathematical model is derived for the *steady two-dimensional magnetohydrodynamic triple diffusive free convection of nanofluid from a vertical stretching sheet*. Separate concentration equations are featured for dual diffusing salts (species 1 and 2) in addition to nanoparticle mass transfer. The Buongiorno two-component nanoscale framework is deployed which also features Brownian motion and thermophoretic body force effects. Soret (thermo-diffusion) and Dufour (diffuso-thermo) effects for both salt species are incorporated. Following non-dimensionalization and transformation of the governing boundary layer equations and associated wall and free stream conditions, the resulting 11^{th} order nonlinear ordinary differential boundary value problem is

solved numerically with MATLAB's bvp4c code. The effects of the emerging parameters e. g. magnetic field parameter, thermal buoyancy parameter, Brownian motion parameter, thermophoresis parameter, modified Dufour parameters of salt 1 and 2, modified Lewis number for salt 1 and 2 etc, on velocity, temperature and all three concentration distributions are plotted and discussed.

2 Governing equations:

Consider the steady two-dimensional heat and mass transfer in boundary layer flow of an incompressible electrically conducting nanofluid (magnetic nanopolymer) from a perforated stretching vertical surface, with two different salts diffusing in the nanofluid with different properties. A variable magnetic field $B(x) = B_o x^{(n-1)/2}$ is applied normal to the vertical surface. It is assumed that the surface is in contact with hot nanofluid at temperature T_f which provides a variable heat transfer coefficient $h_f(x)$.

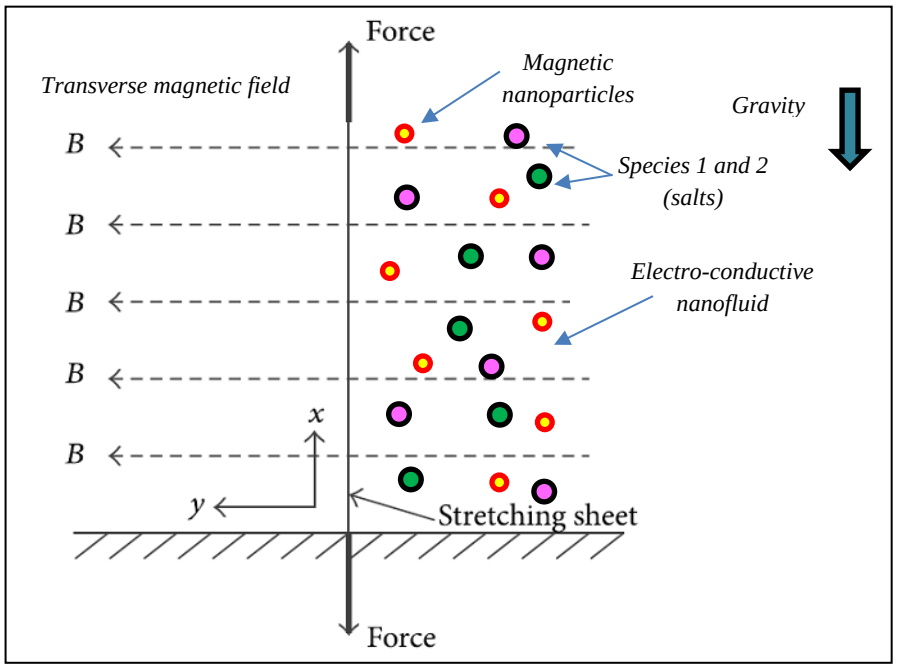

Figure 1: Schematic of magnetic nano-polymer stretching flow regime with coordinate system

Keeping the origin fixed, two equal and opposite forces are applied along the x-axis to stretch the nano-polymer It is assumed that the stretching velocity is in the form of $u_w(x) = ax^n$, where *a* and *n* are constants. The induced magnetic field is neglected in comparison to the applied magnetic field (magnetic Reynolds number is sufficiently small). There is no external electrical field and therefore the impact of polarization of charges is negligibly small. In order to prevent nanoparticles and salts from agglomeration or deposition, it is assumed that the

nanoparticles and both salts are dilutely suspended in the nanofluid. It is also assumed that the Oberbeck-Boussinesq approximation is valid and the mixture of nanofluid and salts is homogenous and is in local thermal equilibrium. In addition, the thermal energy equations include regular diffusion and cross-diffusion terms for both components of salts having concentration,$C_1$and C_2. Following Rionero [41], we assume that two different chemical components ("salts") S_m(m=1,2) have dissolved in the fluid saturated porous medium, which have concentrations $C_m(m = 1,2)$ respectively. The governing conservation equations subject to the Boussinesq approximation, the boundary-layer assumptions, and the other assumptions can be written extending previous studies [16, 18] to consider triple diffusion, magnetic field and Soret-Dufour effects, as follows:

$$\frac{\partial U}{\partial x}+\frac{\partial V}{\partial y}=0 \tag{1}$$

$$U\frac{\partial U}{\partial x}+V\frac{\partial U}{\partial y}=\upsilon\frac{\partial^2 U}{\partial y^2}-\frac{\sigma B^2(x)U}{\rho_{f\infty}}+\left[\begin{array}{l}(1-C_\infty)\rho_{f\infty}\left\{\begin{array}{l}g\beta_T(T-T_\infty)+g\beta_{C_1}(C_1-C_{1\infty})+\\ g\beta_{C_2}(C_2-C_{2\infty})\end{array}\right\}\\ -(\rho_p-\rho_{f\infty})(C-C_\infty)g\end{array}\right] \tag{2}$$

$$U\frac{\partial T}{\partial x}+V\frac{\partial T}{\partial y}=\alpha\frac{\partial^2 T}{\partial y^2}+\tau\left[D_B\left(\frac{\partial C}{\partial y}\right)\left(\frac{\partial T}{\partial y}\right)+\frac{D_T}{T_\infty}\left(\frac{\partial T}{\partial y}\right)^2\right]+\sigma\left[D_{TC_1}\frac{\partial^2 C_1}{\partial y^2}+D_{TC_2}\frac{\partial^2 C_2}{\partial y^2}\right] \tag{3}$$

$$U\frac{\partial C_1}{\partial x}+V\frac{\partial C_1}{\partial y}=D_{S_1}\frac{\partial^2 C_1}{\partial y^2}+D_{C_1T}\frac{\partial^2 T}{\partial y^2} \tag{4}$$

$$U\frac{\partial C_2}{\partial x}+V\frac{\partial C_2}{\partial y}=D_{S_2}\frac{\partial^2 C_2}{\partial y^2}+D_{C_2T}\frac{\partial^2 T}{\partial y^2} \tag{5}$$

$$U\frac{\partial C}{\partial x}+V\frac{\partial C}{\partial y}=D_B\frac{\partial^2 C}{\partial y^2}+\frac{D_T}{T_\infty}\frac{\partial^2 T}{\partial y^2} \tag{6}$$

Here U and V are velocity components in the x and y directions i. e. along and transverse to the vertical stretching surface, respectively, υ is the kinematic viscosity, σ is the electrical conductivity of the nanopolymer, $\rho_{f\infty}$ is the nanopolymer density, g is the acceleration due to gravity, β_T is the coefficient of volumetric thermal expansion of the fluid, β_{C_1} and β_{C_2} are the volumetric solutal expansion coefficients of the nanofluid, α is the thermal diffusivity, τ is

the ratio between the effective heat capacity of the nanoparticle material and heat capacity of the fluid, D_B is the Brownian diffusion coefficient, D_T is the thermophoretic diffusion coefficient, T_∞ is the ambient temperature, D_{TC_1} and D_{TC_2} are solutal Dufour diffusivities, D_{S_1} and D_{S_2} are solutal diffusivities of porous medium, D_{C_1T} and D_{C_2T} are solutal Soret diffusivities, C_1 and C_2 are solutal concentration of species (salts 1 and 2), C is the nanoparticle volume fraction , T is the nanofluid temperature. The corresponding boundary conditions imposed at the wall and in the free stream, are as follows:

$$U = U_W(x), \qquad V = V_W, \qquad -K\frac{\partial T}{\partial y} = h_f(x)(T_f - T)$$

$$C_1 = C_{1W}, \qquad C_2 = C_{2W}, \qquad D_B\left(\frac{\partial C}{\partial y}\right) + \frac{D_T}{T_\infty}\left(\frac{\partial T}{\partial y}\right) = 0 \qquad \text{at } y = 0 \tag{7}$$

$$U \to 0, \qquad \frac{\partial U}{\partial y} \to 0, \qquad T \to T_\infty, \qquad C_1 \to C_{1\infty},$$

$$C_2 \to C_{2\infty}, \qquad C \to C_\infty \qquad \text{as} \quad y \to \infty \tag{8}$$

Introducing a dimensional stream function ψ and the following similarity variables:

$$\eta = \sqrt{\frac{U_W}{\upsilon x}}y \qquad , \ \theta(\eta) = \frac{T - T_\infty}{T_f - T_\infty}, \qquad \psi(x,\eta) = \sqrt{U_w \upsilon x}\, f(\eta)$$

$$\chi_1(\eta) = \frac{C_1 - C_{1\infty}}{C_{1w} - C_{1\infty}}, \qquad \chi_2(\eta) = \frac{C_2 - C_{2\infty}}{C_{2w} - C_{2\infty}}, \qquad \phi(\eta) = \frac{C - C_\infty}{C_w - C_\infty} \tag{9}$$

Where $U = \frac{\partial \psi}{\partial y}$ and $V = -\frac{\partial \psi}{\partial x}$ are the Cauchy-Riemann equations.

Using the similarity transformations (9), the continuity equation (1) is automatically satisfied, and the momentum, energy and triplet of concentration equations are transformed into dimensionless, coupled ordinary (similarity) differential equations as follows:

$$f''' + \left(\frac{n+1}{2}\right)ff'' - n(f')^2 - Mn(f') + \lambda\left[\theta + Nc_1\chi_1 + Nc_2\chi_2 - Nr\phi\right] = 0 \tag{10}$$

$$\theta''(\eta) + \left(\frac{n+1}{2}\right)\left(\frac{\upsilon}{\alpha}\right)f\theta' + Nb(\phi')\theta' + Nt(\theta')^2 + Nd_1\chi_1'' + Nd_2\chi_2'' = 0 \tag{11}$$

$$\chi_1''(\eta)+\left(\frac{n+1}{2}\right)Le_1 f\chi_1'+Ld_1\theta''=0 \tag{12}$$

$$\chi_2''(\eta)+\left(\frac{n+1}{2}\right)Le_2 f\chi_2'+Ld_2\theta''=0 \tag{13}$$

$$\phi''(\eta)+\left(\frac{n+1}{2}\right)Ln f\phi'+\frac{Nt}{Nb}\theta''=0 \tag{14}$$

The corresponding boundary conditions emerge as follows-

$$f'(\eta)=1,\qquad f(\eta)=f_w\ ,\quad \theta'(0)=-A[1-\theta(0)]$$

$$\chi_1(0)=1,\qquad \chi_2(0)=1\ ,\qquad Nb\,\phi'(0)+Nt\,\theta'(0)=0 \qquad \text{at}\ \ \eta=0 \tag{15}$$

$$f'(\eta)\to 0,\qquad f''(\eta)\to 0,\qquad \theta(\eta)\to 0$$

$$\chi_1(\eta)\to 0,\qquad \chi_2(\eta)\to 0,\qquad \phi(\eta)\to 0 \qquad \text{as}\ \ \eta\to\infty \tag{16}$$

The physical quantities used in Equations (10) - (14) are defined as follows: $Mn=\dfrac{\sigma B_o^2}{\left(\rho_{f\infty}\right)\alpha}$ is the magnetic field parameter, $\lambda=\dfrac{g\beta_T\left(T_f-T_\infty\right)x}{\alpha^2x^{2n-1}x}=\dfrac{Gr_x}{\mathrm{Re}_x^2}$ is the thermal buoyancy parameter (in which $Gr_x=\dfrac{g\beta_T\left(T_f-T_\infty\right)x^3}{\upsilon^2}$ is the thermal Grashof number, $\mathrm{Re}_x=\dfrac{u_w x}{\upsilon}$ is the local Reynolds number), $Nc_1=\dfrac{\beta_{C_1}\left(C_{1w}-C_{1\infty}\right)}{\beta_T\left(T_f-T_\infty\right)}$ and $Nc_2=\dfrac{\beta_{C_2}\left(C_{2w}-C_{2\infty}\right)}{\beta_T\left(T_f-T_\infty\right)}$ are the buoyancy ratios for salt 1 and 2, $Nr=\dfrac{\left(\rho_p-\rho_{f\infty}\right)\left(C_w-C_\infty\right)}{\beta_T\left(T_f-T_\infty\right)\left(1-C_\infty\right)\rho_{f\infty}}$ is the nanofluid buoyancy ratio, $Nb=\dfrac{\tau D_B\left(C_w-C_\infty\right)}{\alpha}$ and $Nt=\dfrac{\tau D_T\left(T_f-T_\infty\right)}{\alpha T_\infty}$ are Brownian motion and thermophoresis parameters, $Nd_1=\dfrac{\sigma D_{TC_1}\left(C_{1w}-C_{1\infty}\right)}{\alpha\left(T_f-T_\infty\right)}$ and $Nd_2=\dfrac{\sigma D_{TC_2}\left(C_{2w}-C_{2\infty}\right)}{\alpha\left(T_f-T_\infty\right)}$ are the modified Dufour parameters of salt 1 and 2, $Le_1=\dfrac{\upsilon}{D_{S_1}}$ and $Le_2=\dfrac{\upsilon}{D_{S_2}}$ are the regular Lewis numbers of salt 1 and

2, $Ld_1 = \dfrac{D_{C_1T}\left(T_f - T_\infty\right)}{D_{S_1}\left(C_{1w} - C_{1\infty}\right)}$ and $Ld_2 = \dfrac{D_{C_2T}\left(T_f - T_\infty\right)}{D_{S_2}\left(C_{2w} - C_{2\infty}\right)}$ are the Dufour-solutal Lewis numbers of salt 1 and 2, $Ln = \dfrac{\upsilon}{D_B}$ is the nanofluid Lewis number, $A = \dfrac{1}{K}\sqrt{\dfrac{\upsilon}{a}}h_f\left(x\right)x^{\frac{1-n}{2}}$ is a convective heating parameter, $U_w(x) = ax^n$ is power-law stretching velocity, $B(x) = B_o x^{\frac{n-1}{2}}$ is magnetic field, $V_W(x) = -f_W\sqrt{a\upsilon}\left(\dfrac{n+1}{2}\right)x^{\frac{n-1}{2}}$ is the suction/injection velocity in which f_w is dimensionless lateral mass flux parameter ($f_w > 0$ for suction and $f_w < 0$ for injection).

3 Numerical Solution:

The bvp4c method in MATLAB is used to solve Eqs. (9)- (13) with boundary conditions (14). A 4th order Runge-Kutta quadrature method is deployed with shooting. The first step is to write the ODEs as a system of first order ODEs. The basic idea is to introduce new variables, one for each variable in the original problem plus one for each of its derivative up to one less than the highest derivative appearing. The procedure is outlined in **Fig 2**. Further details are available in [45-47].

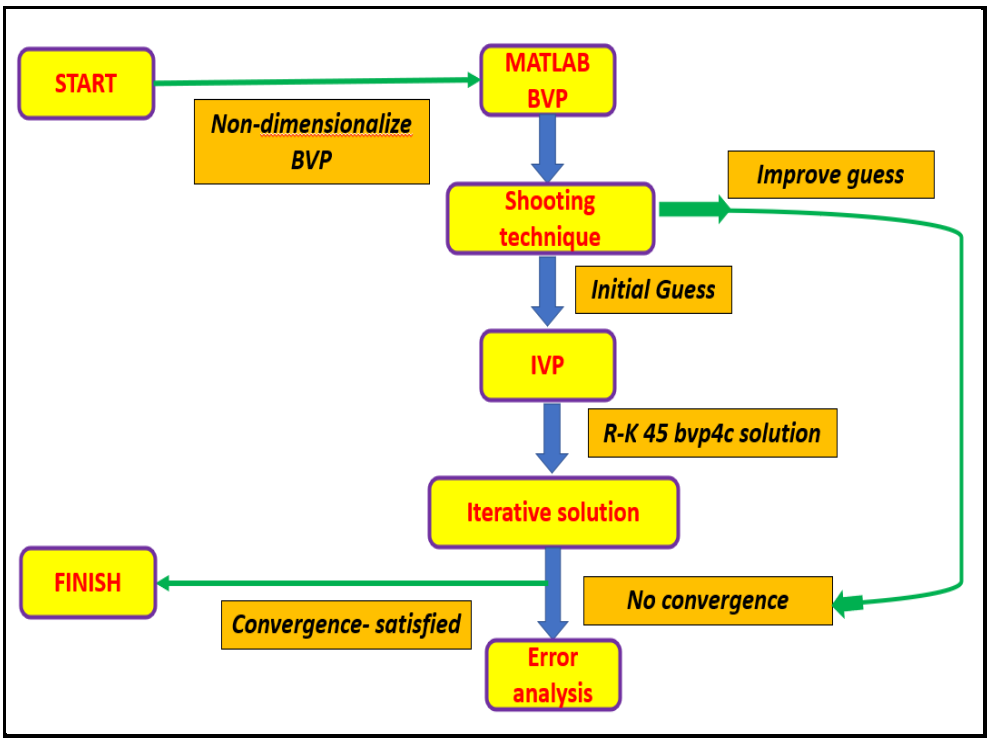

Fig. 2: MATLAB bvp4c numerical procedure

4 Results and Discussion:

Extensive computations have been conducted using the bvp4c MATLAB code. Figs. 3-26 visualize the effects of all key parameters on the velocity f', temperature θ, nanoparticle concentration ϕ, and dual solutal concentrations of salt species 1 (χ_1) and salt 2 (χ_2). In the simulations, n =1 implies linear stretching and $n \neq 1$ corresponds to nonlinear *sheet stretching rates.* All data has been extracted from verified references to represent real nanofluid flows.

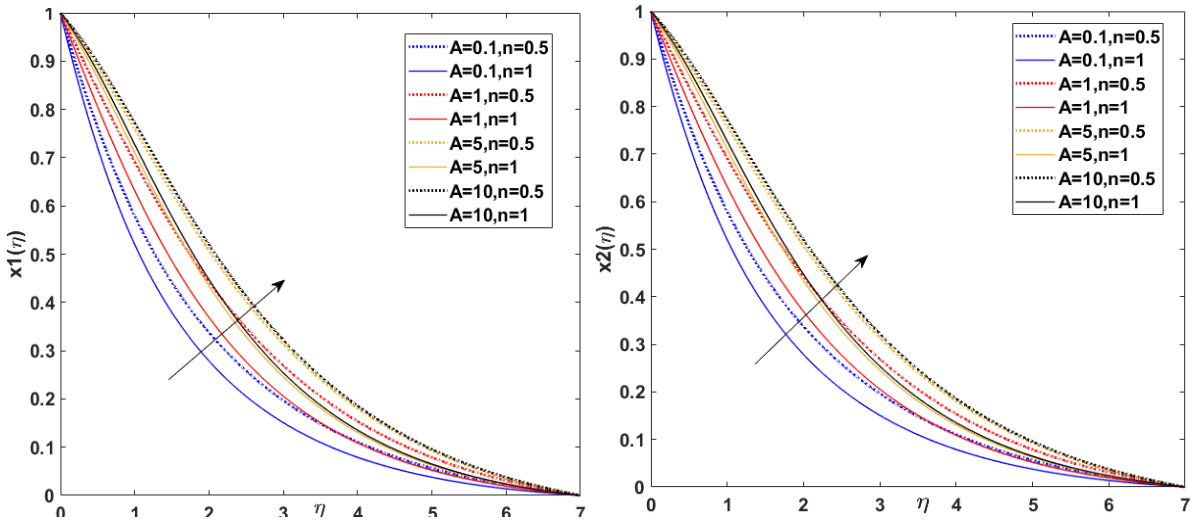

Figure 3: Effect of convective parameter 'A' on solutal concentrations of (a) salt 1 and (b) salt 2

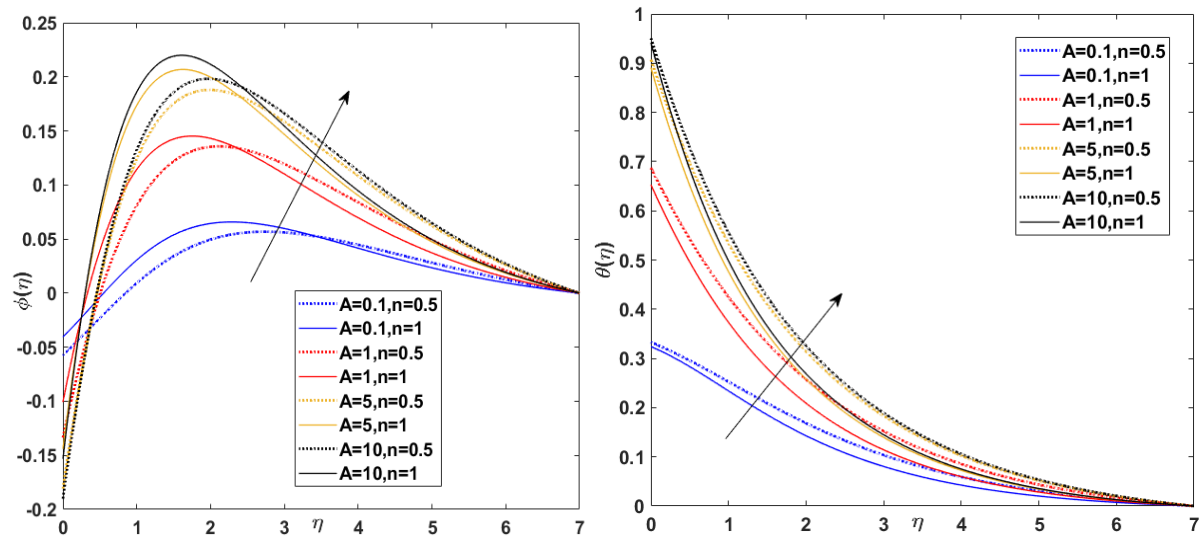

Figure 4: Effect of convective parameter 'A' on dimensionless (a) nanoparticle concentration and (b) temperature

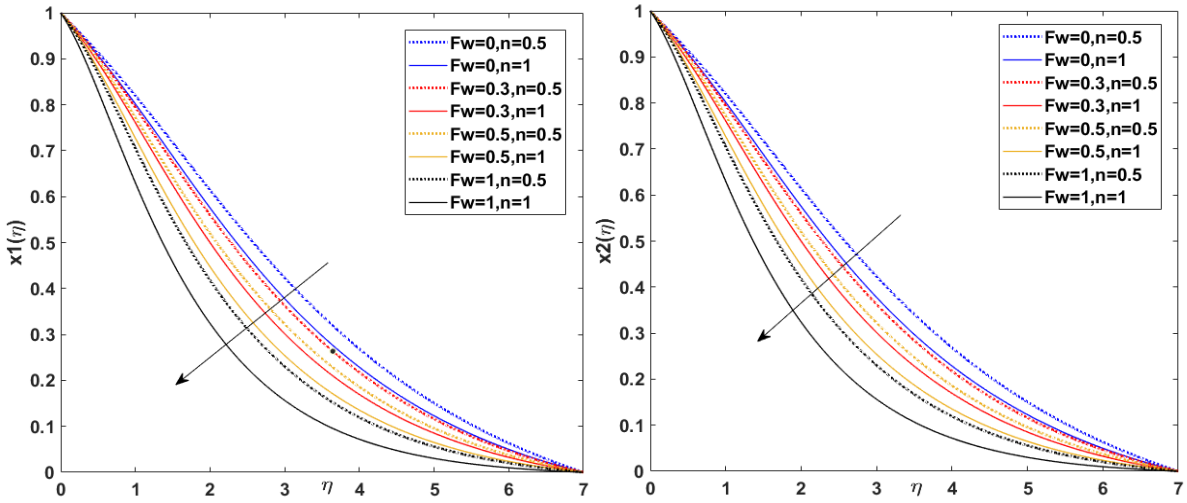

Figure 5: Effect of suction/injection 'f_w' on solutal concentrations of (a) salt 1 and (b) salt 2

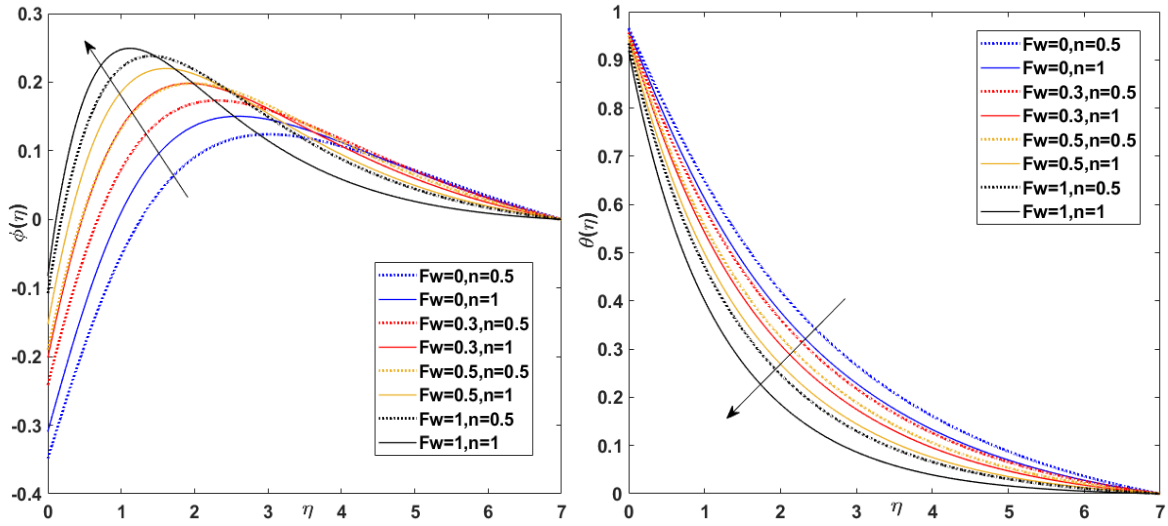

Figure 6: Effect of suction/injection 'f_w' on dimensionless (a) nanoparticle concentration and (b) temperature

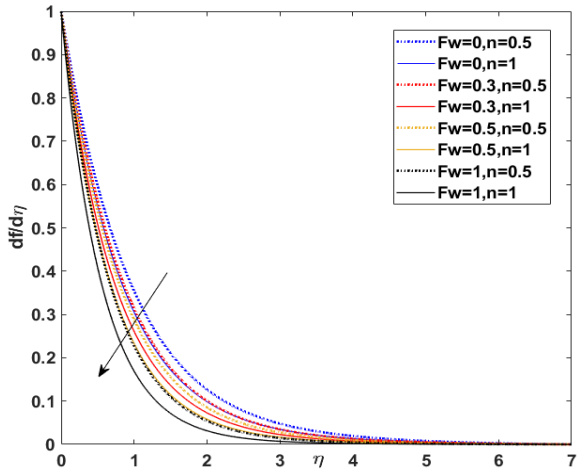

Figure 7: Effect of suction/injection function 'f_w' on dimensionless velocity

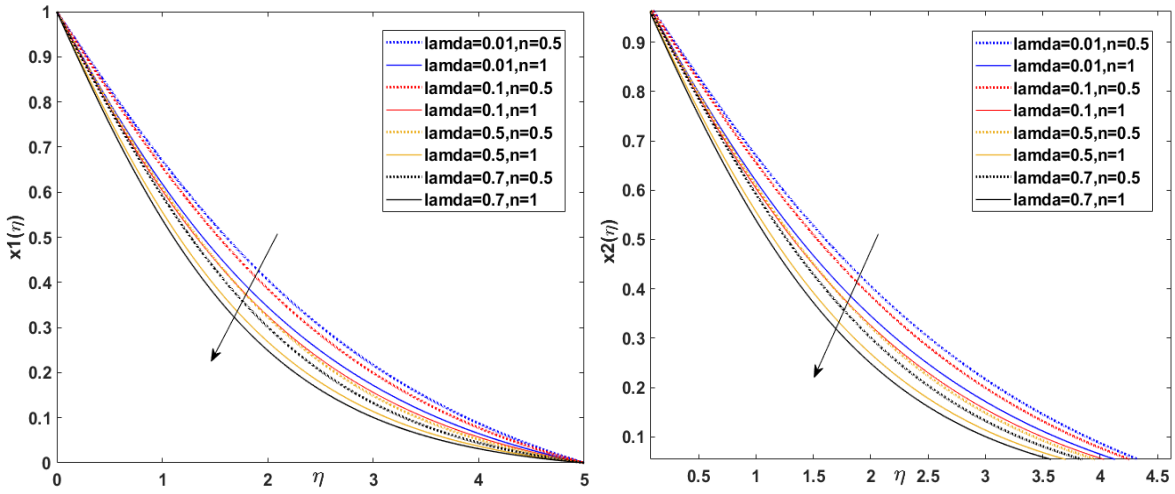

Figure 8: Effect of buoyancy parameter 'λ' on solutal concentrations of (a) salt 1 (b) salt 2

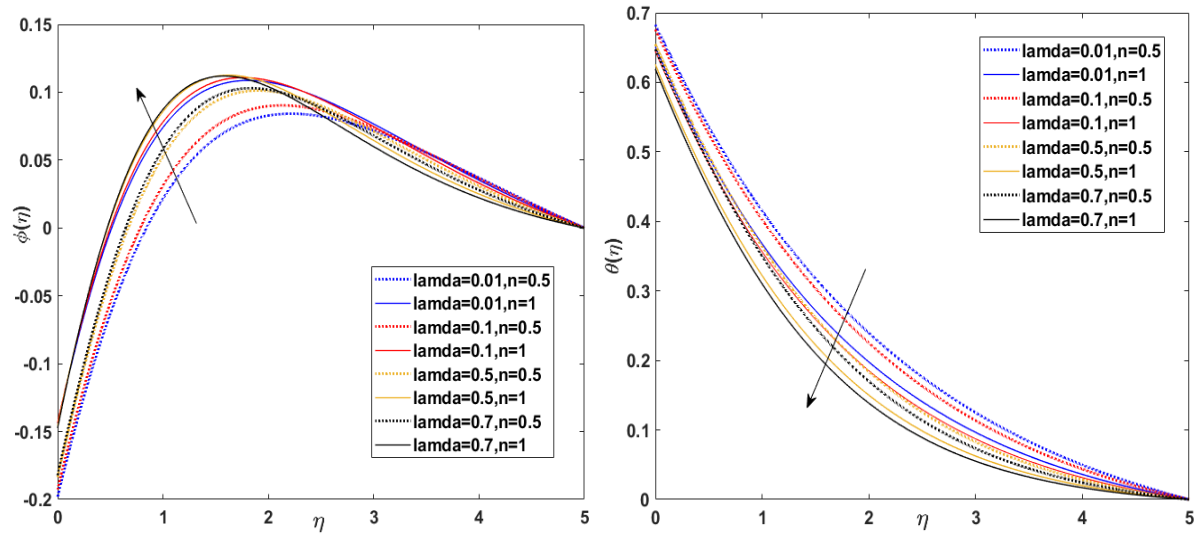

Figure 9: Effect of buoyancy parameter 'λ' on dimensionless (a) nanoparticle concentration (b) temperature

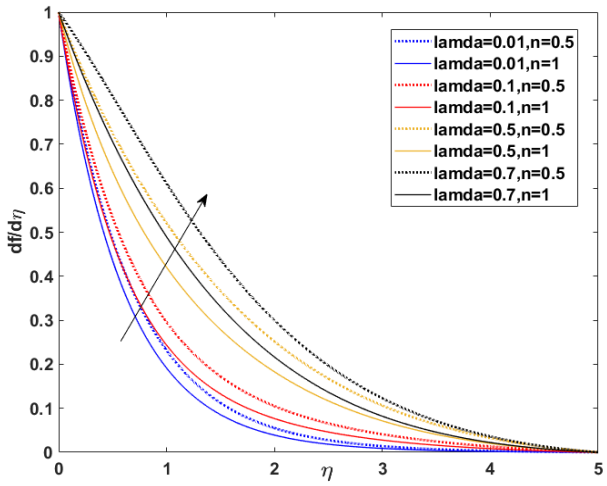

Figure 10: Effect of thermal buoyancy parameter 'λ' on dimensionless velocity

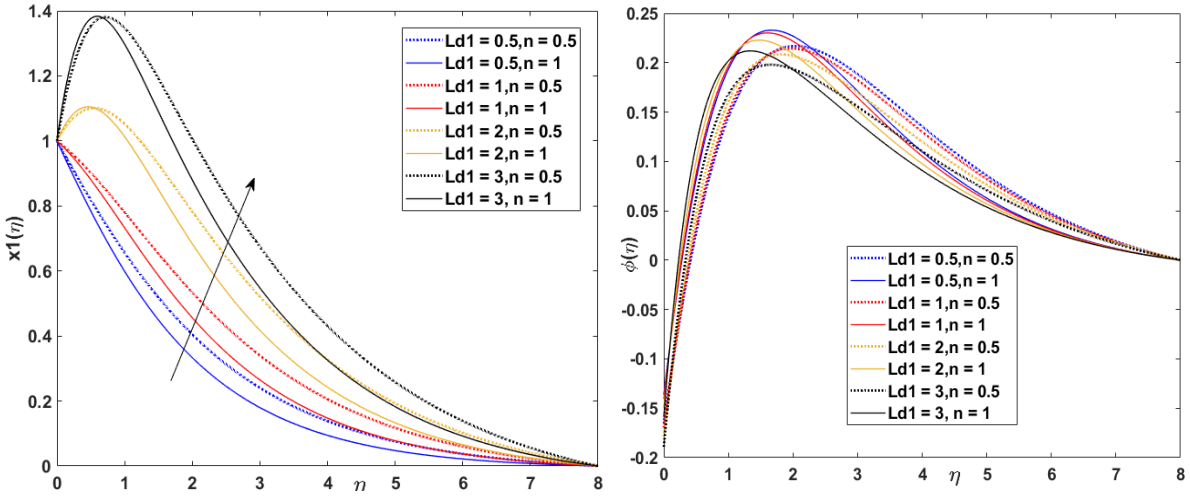

Figure 11: Effect of Dufour solutal Lewis number of salt 1 'Ld_1' on (a) solutal concentrations of salt 1 and (b) dimensionless nanoparticle concentration

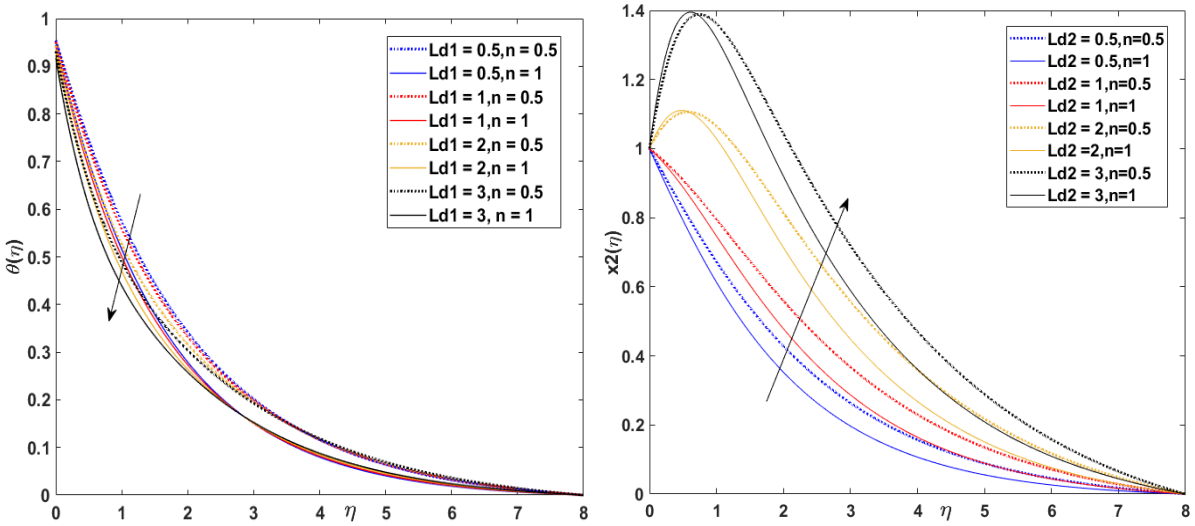

Figure 12: Effect of (a) Dufour solutal Lewis number of salt 1 'Ld_1' on temperature and (b) Dufour solutal Lewis number of salt 2 'Ld_2' on solutal concentrations of salt 2

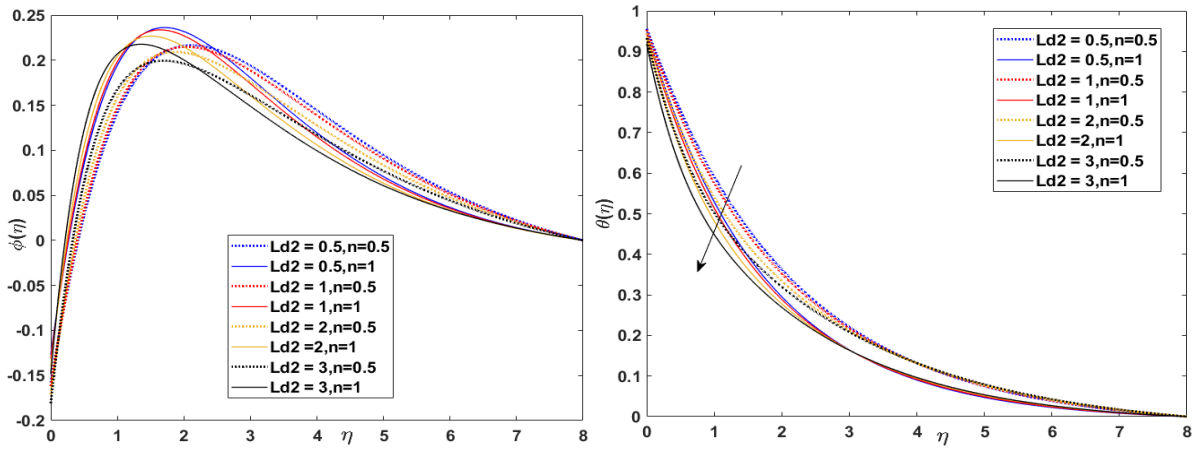

Figure 13: Effect of Dufour solutal Lewis number of salt 2 'Ld_2' on (a) dimensionless nanoparticle concentration and (b) dimensionless temperature

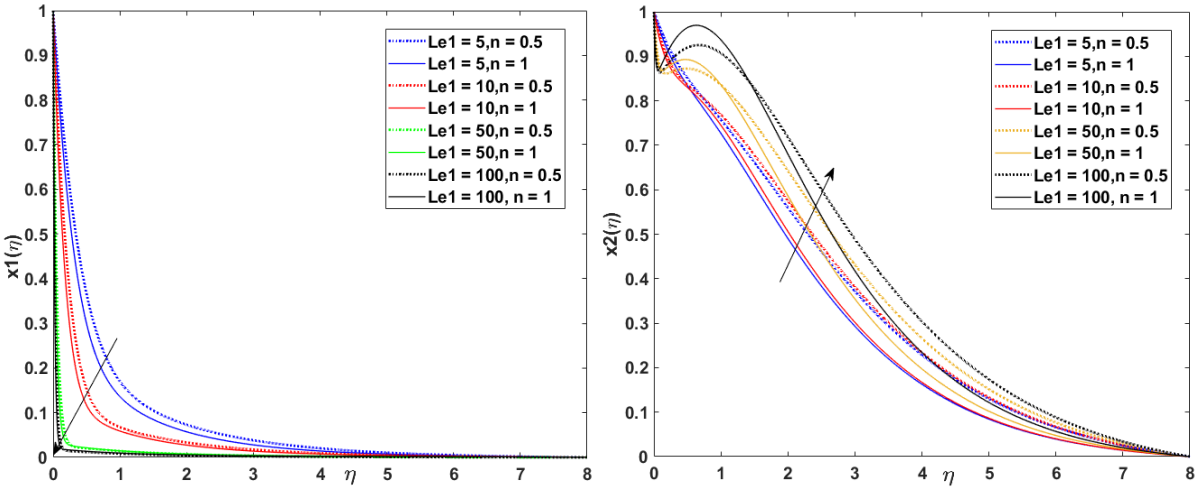

Figure 14: Effect of regular Lewis number of salt 1 'Le_1' on solutal concentrations of (a) salt 1 and (b) salt 2

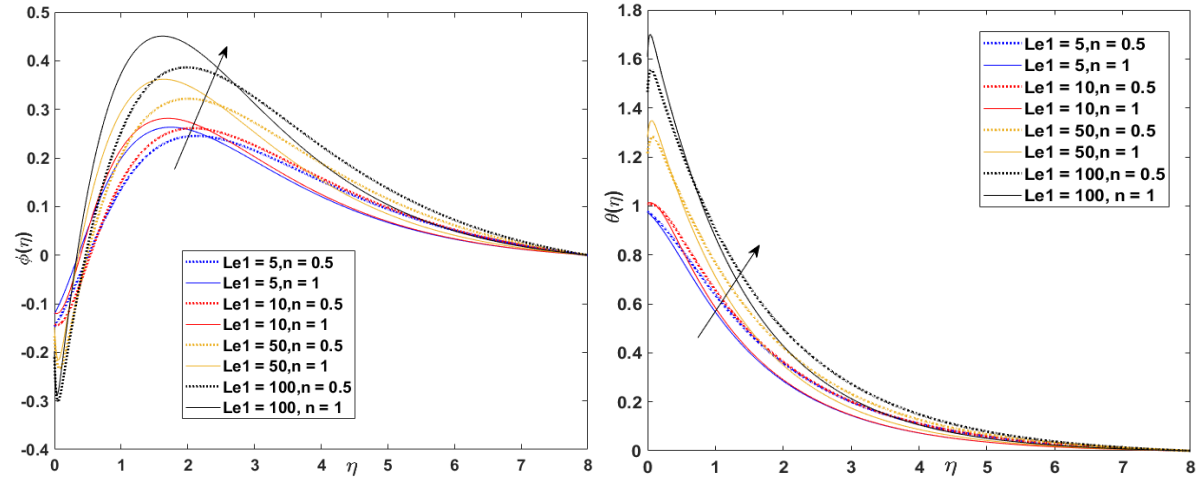

Figure 15: Effect of regular Lewis number of salt 1 'Le_1' on dimensionless (a) nanoparticle concentration and (b) temperature

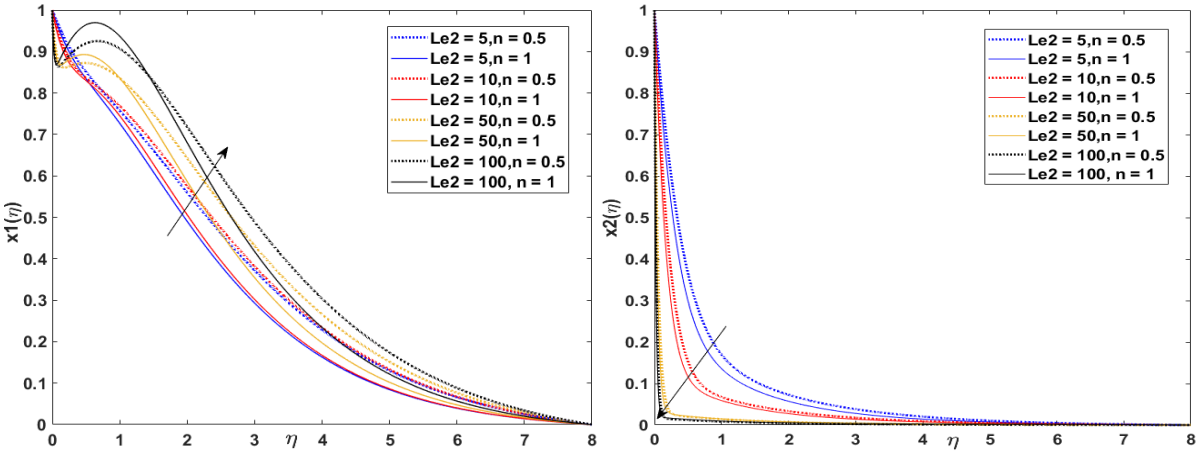

Figure 16: Effect of regular Lewis number of salt 2 'Le_2' on solutal concentrations of (a) salt 1 and (b) salt 2

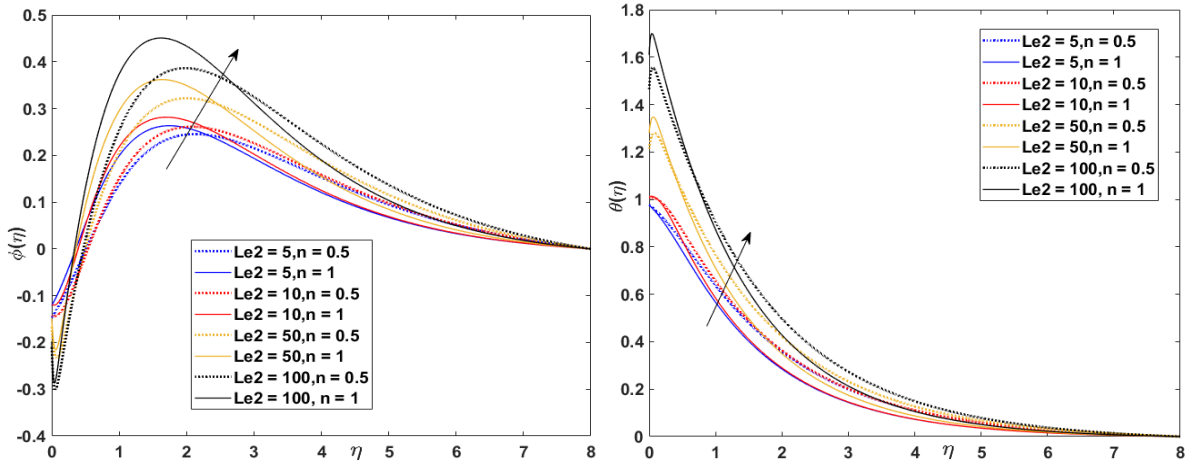

Figure 17: Effect of regular Lewis number of salt 2 'Le_2' on dimensionless (a) nanoparticle concentration and (b) temperature

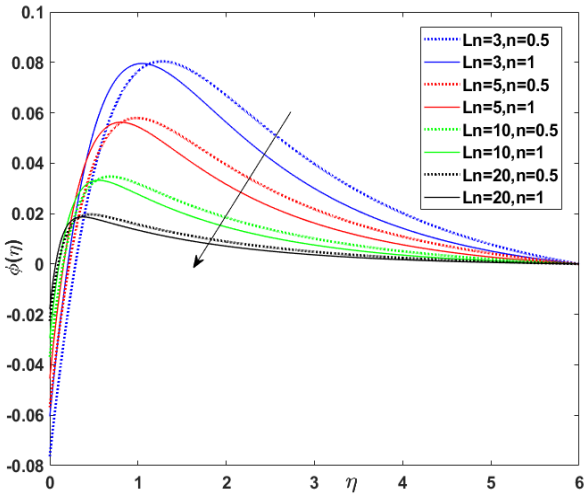

Figure 18: Effect of nanofluid Lewis number 'Ln' on dimensionless nanoparticle concentration

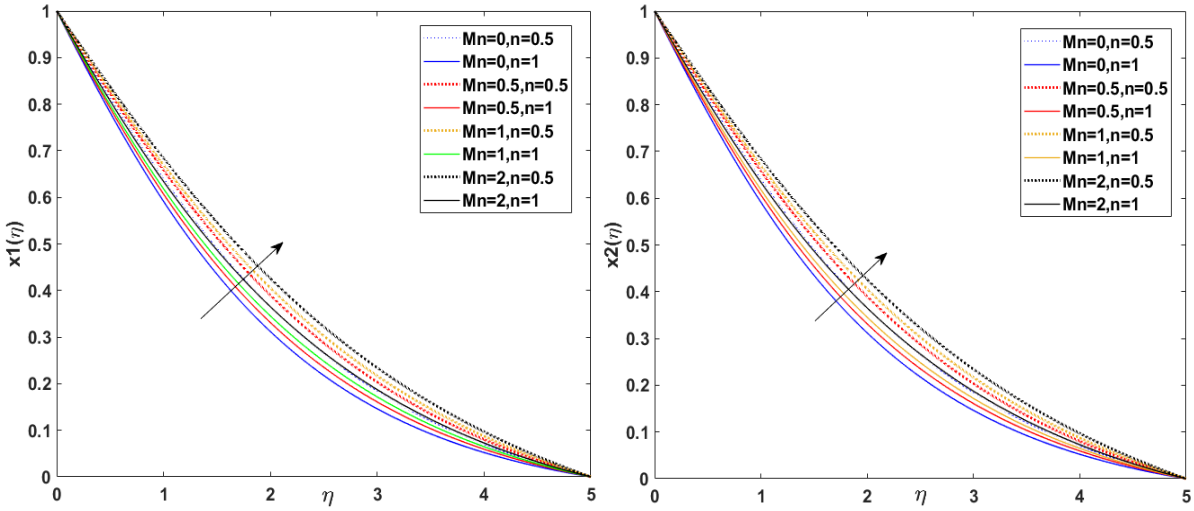

Figure 19: Effect of magnetic field parameter 'Mn' on solutal concentrations of (a) salt 1, (b) salt 2

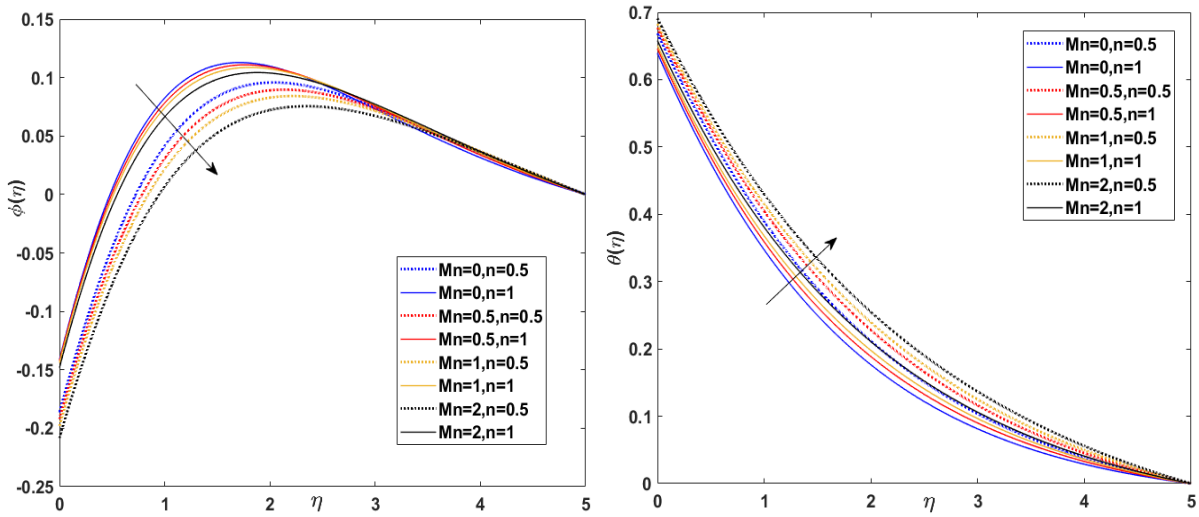

Figure 20: Effect of magnetic field parameter 'Mn' on dimensionless (a) nanoparticle concentration and (b) temperature

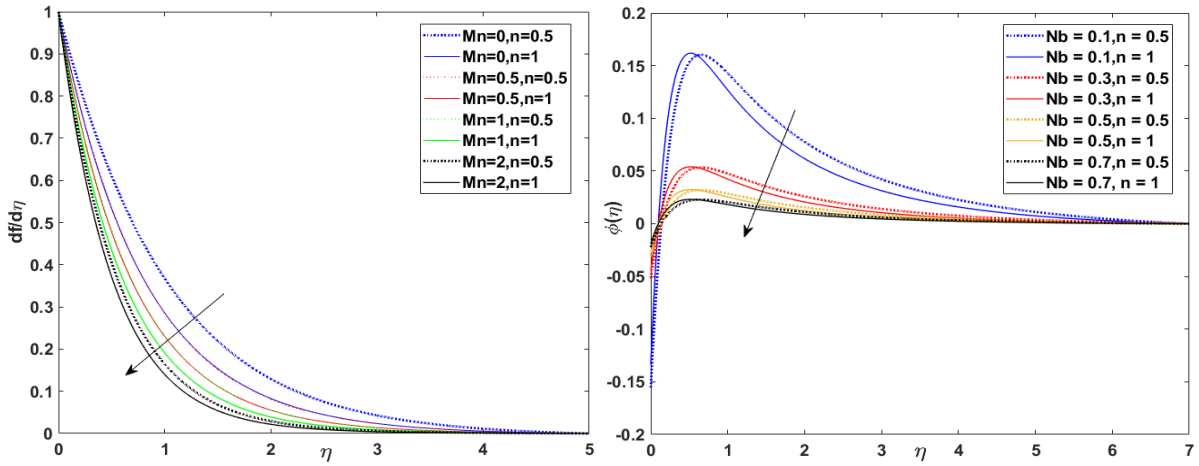

Figure 21: Effect of (a) magnetic field parameter 'Mn' on dimensionless velocity and (b) Brownian motion parameter 'Nb' on nanoparticle concentration

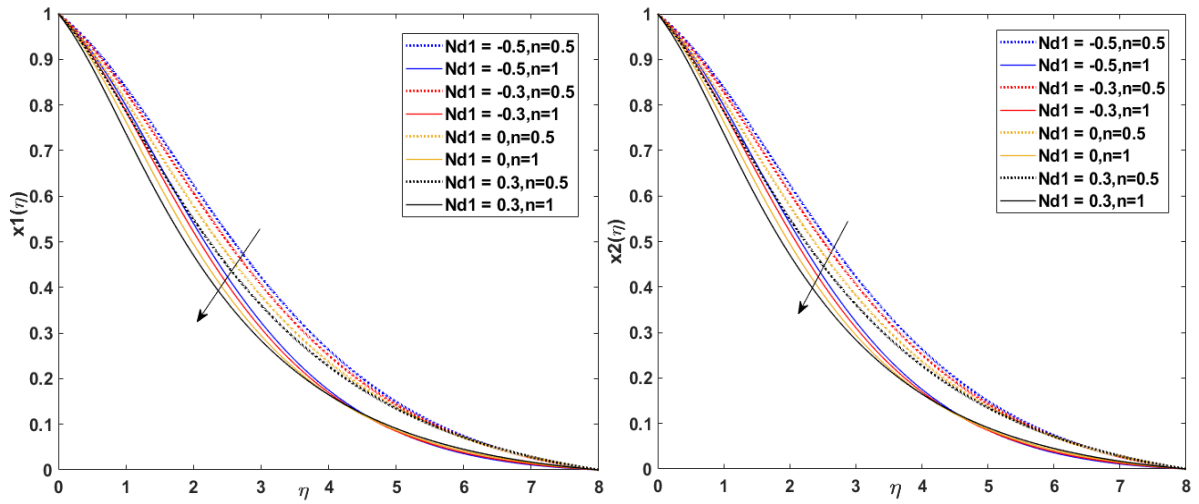

Figure 22: Effect of modified Dufour parameter of salt 1 'Nd_1' on solutal concentrations of (a) salt 1 and (b) salt 2

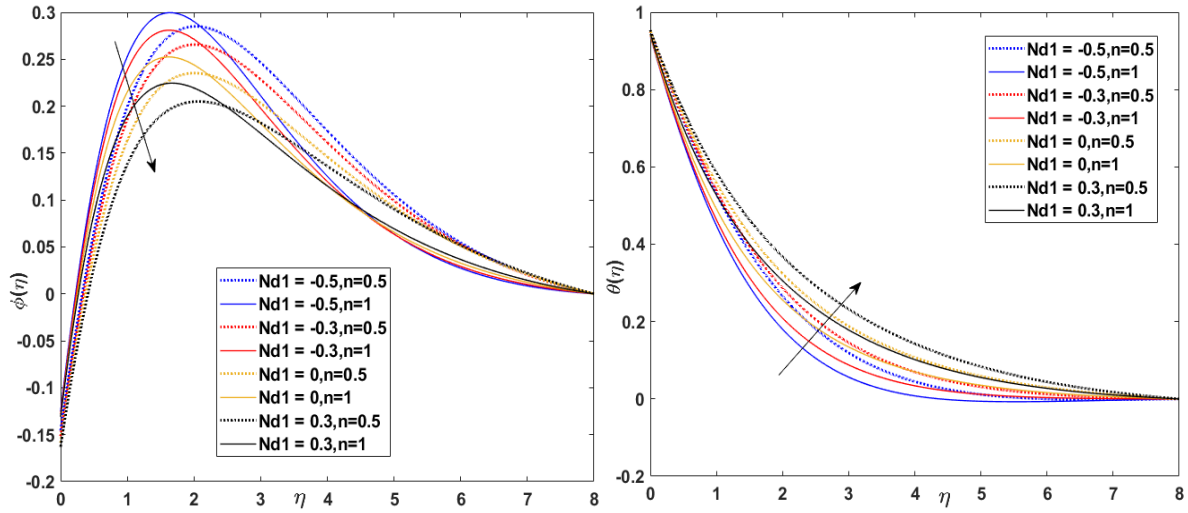

Figure 23: Effect of modified Dufour parameter of salt 1 'Nd_1' on dimensionless (a) nanoparticle concentration and (b) temperature

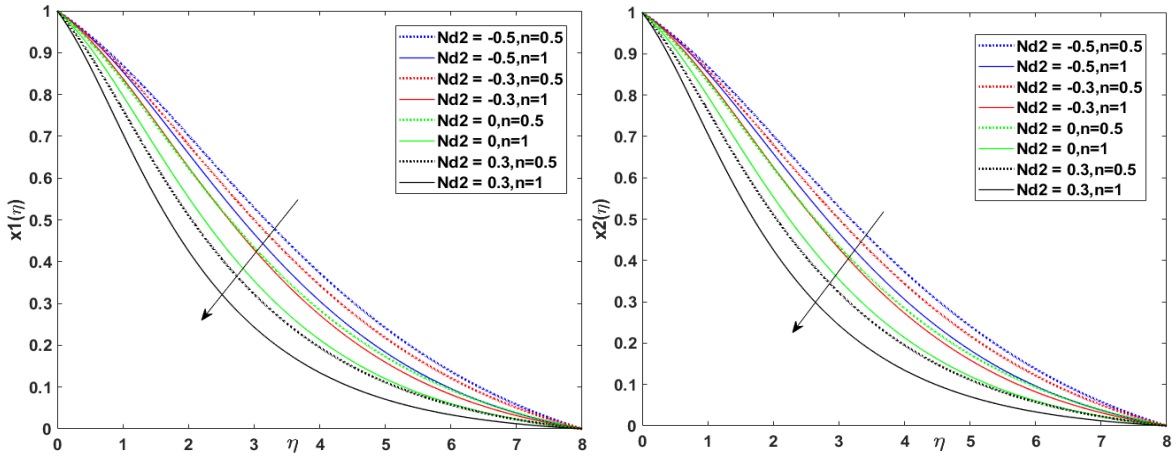

Figure 24: Effect of modified Dufour parameter of salt 2 'Nd_2' on solutal concentrations of (a) salt 1 and (b) salt 2

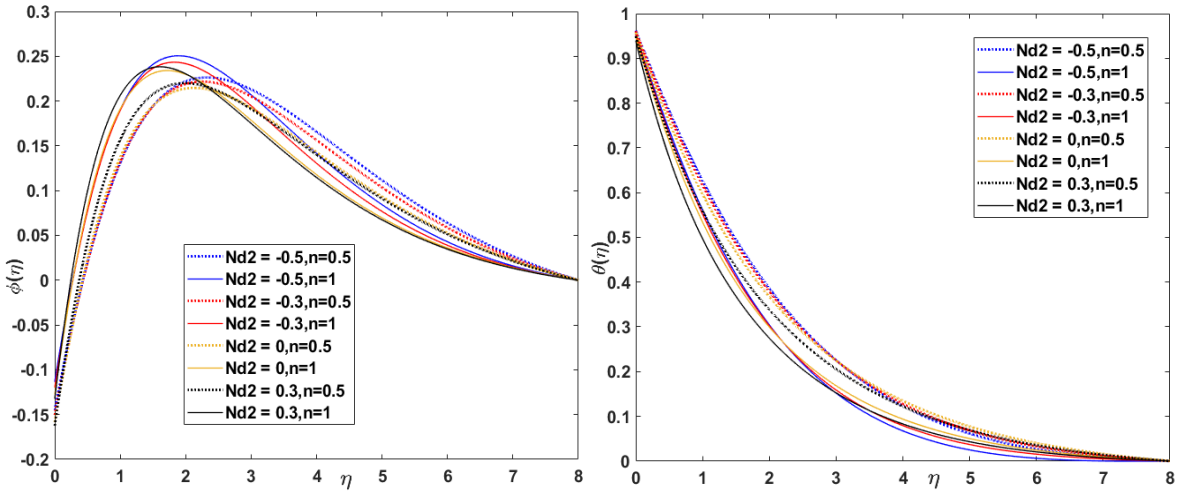

Figure 25: Effect of modified Dufour parameter of salt 2 'Nd_2' on dimensionless (a) nanoparticle concentration and (b) temperature

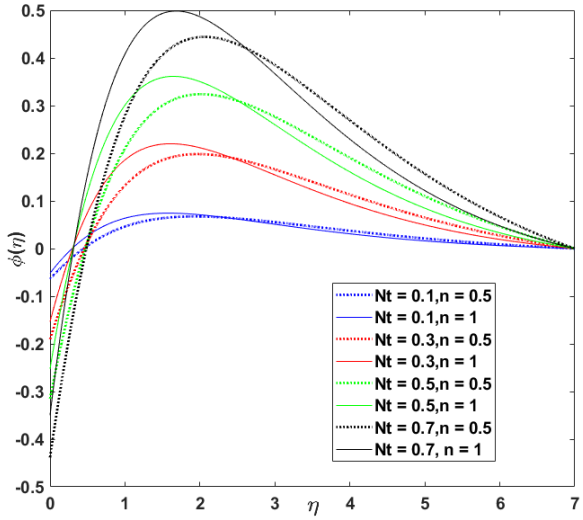

Figure 26: Effect of thermophoresis parameter 'Nt' on dimensionless nanoparticle concentration

In all the plots we consider linear and nonlinear stretching (*0.5 < n< 1.0*), with variation of an individual different parameter also.

Fig. 3 visualizes the impact of convective parameter 'A' and stretching rate, *n*, on solutal concentrations of (a) salt 1 and (b) salt 2. $A = \frac{1}{K}\sqrt{\frac{\upsilon}{a}} h_f(x) x^{\frac{1-n}{2}}$ and arises in the modified wall boundary condition for temperature, in Eqn. (15), viz $\theta'(0) = -A[1-\theta(0)]$. Temperature is strongly coupled in Eqn. (11) to both the salt species concentration equations (12, 13) via the terms $+Nd_1\chi_1'', +Nd_2\chi_2''$. The salt concentration equations are also coupled to the temperature equation via the terms $+Ld_1\theta''$ and $+Ld_2\theta''$. There is therefore a very strong interplay between the temperature and salt concentration fields. The increment in *A* boosts the solutal concentrations of salt species 1 (χ_1) and salt 2 (χ_2). In other words, convective heating at the wall encourages the diffusion of both salt species in the boundary layer of the nanopolymer. This will manifest in a boost in both salt 1 and salt 2 concentration boundary layer thicknesses also. It is also noteworthy that for the nonlinear stretching case (dotted line, n = 0.5) consistently higher magnitudes for both solute concentrations are computed. Lower values are associated with the linear stretching case (solid line, n = 1). Asymptotically smooth decays are obtained in the free stream confirming the selection of an adequately large infinity boundary condition in the MTALAB bvp4c solver. Maximum solute concentrations are always computed at the wall for any value of *A and n.* Furthermore, slightly greater magnitudes of salt

2 concentration are computed over the same range of *A and n values*, and this is associated with the higher molecular diffusivity of this second solute.

Fig. 4 displays the evolution in (a) nanoparticle concentration and (b) temperature with variation in convective parameter '*A*' and stretching rate, *n*. The direct proportionality of the convective wall parameter A to the convection heat transfer coefficient (h_f) generates a strong heating effect. Although initially there is a delay in the nanoparticle concentration; however close to the wall (stretching sheet) a strong enhancment is observed in magnitudes with increment in *A*. This trend is sustained for some distance into the boundary layer attaining a peak value and thereafter a monotnic descent into the free stream is computed (Fig 4a). The coupling of the nanoparticle diffusion equation (14) to the energy equation (11) via the nanoscale term, $+\frac{Nt}{Nb}\theta''$ enables the nanoparticle diffusion to be influenced by thermal effects. Generally nanoparticle concentration boundary layer thickness is accentuated with increasing convective heating parameter (A). closer to the wall nonlinear stretching (n = 0.5) relative to lienar stretching (n = 1) damps the nanoparticle concentration magnitudes; however further from the wall the opposite trend is produced and nonlinear stretching boosts concentration magnitudes. Clearly the nature of the forces involved in stretching the sheet exerts a different influence throughout the boundary layer on nanoparticle diffusion a maximum is not computed at the wall), whereas the response is more consistent throughout the boundary layer for the solutal species (salts) as observed in Fig. 3. Fig 4a shows that a strong elevation in temperature is induced with increasing convective parameter which is sustained at all values of the transverse coordinate (η). Maximum temperatures always arise at the wall and nonlinear stretching (n = 0.5) produces a stronger heating effect than linear stretching (n =1) and an associated thicker thermal boundary layer.

Fig. 5 presents the influence of suction/injection parameter 'f_w' on solutal concentrations of (a) salt 1 and (b) salt 2. Only the case of a *solid wall* ($f_w = 0$) and *suction* ($f_w > 0$) are considered. There is a significant reduction computed in both solutal concentrations of salt species 1 (χ_1) and salt 2 (χ_2) with increasing suction effect. In materials processing operations, the removal of material via perforations at the wall inhibits momentum diffusion and this decelerates the boundary layer stretching. This in turn damps the diffusion of salt species and results in thinner salt solute boundary layers. Cleary the solute concentrations are maximized for the solid wall case where suction is absent. There is a strong coupling between the solute (salt) concentration boundary layer Eqns. (12) and (13) with the momentum boundary layer equation (10), via the

terms) $+\left(\frac{n+1}{2}\right)Le_1 f\chi_1{}'$ and $+\left(\frac{n+1}{2}\right)Le_2 f\chi_2{}'$ appearing in the former and the salt species buoyancy terms, $+\lambda[Nc_1\chi_1 + Nc_2\chi_2]$, appearing in the latter. There is therefore a direct influence of velocity field on the salt diffusion processes and this manifests in a strong modification in salt 1 and 2 concentration distributions via the suction/injection wall boundary condition. Again, significantly greater salt 1 and 2 concentrations are achieved with nonlinear stretching (n = 0.5) compared with linear stretching (n = 1). Effectively greater salt 1 and 2 species boundary layer thicknesses will therefore be produced with nonlinear stretching of the nanopolymer.

Fig. 6 shows the distributions for (a) nanoparticle concentration and (b) temperature with variation in wall suction parameter (f_w) and stretching rate, n. There is very near to the wall a strong enhancment in nanoparticle concentration with greater suction effect (values are minimal for the solid wall case, f_w=0). However further from the wall, once maximum magnitudes have been attained, the effect of wall suction reversed and there is a significant depletion thereafter with increasing suction. Closer to the wall linear stretching (n = 1) achieves higher nanoparticle concentration values whereas further way nonlinear stretching (n = 0.5) dominates. There is strong coupling between the momentum equation (10) and the nanoparticle diffusion equation (14) via the term, $+\left(\frac{n+1}{2}\right)Lnf\phi'$ arising in the former and the nanoparticle coupling species buoyancy term, $\lambda[-Nr\phi]$featured in the latter. This produces a great sensitivity in the nanoparticle behaviour to the velocity field which is directly affected by the wall suction boundary condition in Eqn. (15). A delicate interplay between wall suction and sheet stretching is therefore experienced in the nanoparticle diffusion process. Temperature is observed to be strongly suppressed with increasing wall suction and this behaviour is maintained at all locations in the boundary layer. Temperature is influenced by velocity via the convective term, $+\left(\frac{n+1}{2}\right)\left(\frac{\upsilon}{\alpha}\right)f\theta'$ in Eqn. (11) and also the thermal buoyancy coupling term, $\lambda\theta$ in eqn. (10). Nonlinear stretching achieves *higher temperatures* than linear stretching. For the case of a solid wall (f_w=0) temperature is maximized. The implication is that an effective thermal control mechanism is attained via wall suction which is important in regulation of excessive heat in the nanopolymer manufacturing process [14, 27, 29]. Significant cooling can be produced by a simple escalation in wall mass flux via the sheet pores. Linear stretching rate can also assist in this process and simultaneously reduce thermal boundary layer thickness.

Fig. 7 shows the impact of suction/injection function 'f_w' on dimensionless velocity profiles. There is a clear decrement in velocity with greater wall suction. The intensification in wall

suction causes greater adherence of the momentum boundary layer to the wall (stretching sheet). This damps momentum and decelerates the flow and simulatenously reduces momentum boundary layer thickness. Significant flow control is therefore achieved via wall suction. Nonlinear stretching (n = 0.5) conversely accelerates the flow i.e. incerases velocities relative to linear stretching (n = 1).

Fig. 5 presents the influence of thermal buoyancy parameter 'λ' on solutal concentrations of (a) salt 1 (b) salt 2'. $\lambda = \dfrac{g\beta_T\left(T_f - T_\infty\right)x}{\alpha^2 x^{2n-1}x} = \dfrac{Gr_x}{\mathrm{Re}_x^2}$ and provides a quantification of the relative influence of thermal buoyancy in the boundary layer regime and viscous hydrodynamic resistance. Both figures show a substantial depletion induced in solutal concentrations of salt species 1 (χ_1) and salt 2 (χ_2) with increasing thermal buoyancy. Although the parameter λ only features in the single term $\lambda[\theta]$ in the momentum eqn. (10), there is also strong coupling via the Dufour terms (which create an energy flux by virtue of the salt compositional concentration gradient) in the energy eqn. (11). Enhanced intensity of thermal convection currents asociated with stronger thermal buoyancy however damps the diffusion of the salt species. This decreases the salt 1 and 2 concentration boundary layer thicknesses. As in earlier plots, the nonlinear stretching (n = 0.5) produces higher magnitudes of both salt concentrations compared with the linear stretching case (n = 1).

Figure 9 visualizes the response in (a) nanoparticle concentration and (b) temperature with increment in thermal buoyancy parameter, 'λ'. Distinct from the salt species responses computed in Fig. 6, the nanoparticle concentration is enhanced near the wall with increment in thermal buoyancy, λ. The mechanism of nanoparticle diffusion is distinct from that of the salt components. Near the wall nanoparticles are increased in concentration. However further from the wall after the peak nanoparticle concentration has been attained, there is a reduction in concentration magnitudes with stronger thermal buoyancy. Linear stretching accentuates nanoparticle diffusion in clsoe proximity to the wall whereas nonlinear stretching achieves a similar effect further from the wall. Temperature is considerably lowered with increasing 'λ' values. This is precipitated by the mobilization of thermal convection currents under stronger buoyancy which transport greater heat to the surface and drain thermal energy from the boundary layer. Thermal boundary layer thickness is suppressed therefore with stronger thermal buoyancy effect. Consistently nonlinear stretching achieves higher temperatures

throughout the boundary layer domain transverse to the stretching sheet comapred with linear stretching.

Fig. 10 depicts the velocity field response to a change in thermal buoyancy parameter, 'λ'. The synthesis of stronger thermal convection currents in the boundary layer encourages momentum development while suppressing heating. This accelerates the nanopolymer flow and leads to a strong upsurge in velocity magnitudes. At higher buoyancy parameter values (λ ~0.7) closer to the wall, even though the thermal buoyancy force is still exceeded by viscous resistance, a linear decay is computed whereas at weaker λ values the topology of profiles is strongly parabolic. A strong acceleration effect is also induced with nonlinear stretching (n = 0.5) relative to linear stretching (n = 1). Momentum boundary layer thickness is effectively decreased overall with stronger thermal buoyancy and a smaller stretching velocity.

Figure 11 displays the evolution in (a) solutal concentrations of salt 1 and (b) nanoparticle concentration with variation in the Dufour solutal Lewis number of salt 1 'Ld$_1$'. $Ld_1 = \dfrac{D_{C_1T}\left(T_f - T_\infty\right)}{D_{S_1}\left(C_{1w} - C_{1\infty}\right)}$ and is the regular Lewis number of salt 1 and features in the diffuso-thermal term, $+Ld_1\theta''$, in the salt 1 concentration equation (12). Increasing this parameter magnifies the imapct of the temperature gradient on the mass flux of the salt species. This naturally boosts the salt 1 concentration magnitudes and associated species boundary layer thickness. A significant over-shoot in the salt 1 concentration is observed near the wall for Ld_1 > 1. When Ld_1 = 1, the thermal diffusion and salt diffusion rates are equivalent in the regime. When Ld_1 > 1, salt 1 molecular diffusion rate is exceeded by the thermal diffusion rate and this leads to modification in the distributions near the wall. The over shoot is evidently absent for Ld_1 ≤1. Solute 1 concentration values for nonlinear stretching clearly exceed those computed for linear stretching. Concentration boundary layer thickness for salt 1 is therefore maximized with nonlinear stretching and higher Dufour solutal Lewis number. Nanoparticle concentration is initially elevated with increasing Ld_1 values and linear stretching near the wall; however further from the wall the contrary response is observed.

Figure 12 displays the effect of (a) Dufour solutal Lewis number of salt 1 'Ld$_1$' on temperature and (b) Dufour solutal Lewis number of salt 2 'Ld$_2$' on solutal concentrations of salt 2. Increasing Ld$_1$ depletes the temperatur magnitudes and leads to a cooling effect. Thermal boundary layer htickness is reduced (Fig. 12a). Analagous to the salt 1 Dufour solutal Lewis number, the Dufour solutal Lewis number of salt 2 'Ld$_2$' arises in the term $+Ld_2\theta''$ in the salt 2 diffusion equation (13).

$Ld_2 = \dfrac{D_{C_2T}\left(T_f - T_\infty\right)}{D_{S_2}\left(C_{2w} - C_{2\infty}\right)}$ and expresses the relative diffusion rates of heat and salt 2 mass. Higher values of Ld_2 clearly will encourage mass flux of salt 2 and this will boost concentration magnitudes (Fig. 12b) and produce a greater salt 2 concentration boundary layer thickness. The concentration overshoot is similar to that observed for salt 1 (Fig. 11a). The magnitude of salt 2 concentrations is also greater for nonlinear stretching (n = 0.5) compared with linear stretching (n = 1); effectively nonlinear stretching of the vertical sheet will as a result increase the species 2 boundary layer thickness.

Figure 13 shows the evolution in (a) dimensionless nanoparticle concentration and (b) dimensionless temperature, with a change in Dufour solutal Lewis number of salt 2 'Ld_2'. Close to the wall, nanoparticle concentrations are elevated with increment in Ld_2; however further from the wall the pattern of influence is altered and there is a depression in nanoparticle concentrations (Fig. 13a). Temperature (Fig. 13b) is generally depleted with greater Ld_2 values. The dominance of thermal diffusion rate to salt 2 molecular diffusion rate results in a cooling effect in the regime which decreases thermal boundary layer thickness. Linear stretching manifests in a cooling effect relative to nonlinear stretching as it reduces temperatures.

Figure 14 illustrates the impact of regular Lewis number of salt 1 'Le_1' on solutal concentrations of (a) salt 1 and (b) salt 2. $Le_1 = \dfrac{\upsilon}{D_{S_1}}$ and expresses the relative rate of momentum diffusion to salt 1 molecular diffusion. It features in the term, $+\left(\frac{n+1}{2}\right) Le_1 f \chi_1'$ in the salt 1 diffusion equation (12) which couples this equation with the momentum equation (10). Increment in Le_1 markedly depletes the salt 1 concentration magnitudes, χ_1 (Fig. 14a) and reduces the salt 1 concentration boundary layer thickness. A very sharp descent is computed from the wall. Strong inhibition of salt 1 diffusion is therefore induces with a massive increase in Le_1 from 5 to 100. On the other hand in Fig. 14b, χ_2 i.e. salt 2 concentrations although very quickly suppressed very clsoe to the wall with greater salt 1 Lewis number, are dramatically enhanced further from the wall and this is sustained into the free stream. There is therefore a competition between salt 1 and salt 2 flux which can be manipulated by judicious selection of the appropriate salt species to incur different behaviour in the boundary layer. In both salt cases however nonlinear stretching (dotted lines) produces greater concentration magnitudes relative to linear stretching (solid lines), although much higher magnitudes are computed for salt 2.

Figure 15 visualizes the influence of regular Lewis number of salt 1 'Le_1' on dimensionless (a) nanoparticle concentration and (b) temperature. There is a substantive elevation in both nanoparticle concentration and temperature values with greater salt 1 Lewis number. However while peak nanoparticle concentration arises further from the wall, maximum temperatures are always observed at the wall. Initially linear stretching (n =1) results in greater nanoparticle concentrations closer to the stretching surface (wall); however further into the boundary layer higher magnitudes are found to correspond to nonlinear stretching. A similar trend is computed for the temperature profiles. Thermal boundary layer thickness is effectively enhanced with greater salt 1 Lewis number.

Figure 16 depict the effect of regular Lewis number of salt 2 'Le_2' on solutal concentrations of (a) salt 1 and (b) salt 2. This parameter arises in the salt 2 diffusion equation (13) via the term, $+\left(\frac{n+1}{2}\right) Le_2 f \chi_2'$, which couples this equation to the momentum equation (10). The salt 1 concentration, χ_1 is initially suppressed with increment in salt 2 Lewis number, but thereafter is strongly accentuated (Fig 16a). However, the salt 2 concentration is greatly decreased with increment in Le_2. Generally salt 1 concentration boundary layer thickness is therefore boosted whereas salt 2 species boundary layer thickness is elevated. The difference in molecular diffusivities strongly modifies the salt 1 and 2 species diffusion characteristics. Nonlinear stretching effectively reduces both salt species boundary layer thicknesses. Markedly higher magnitudes are computed for salt 1 concentration at any value of salt 2 Lewis number or stretching parameter.

Figure 17 illustrates the evolution in (a) nanoparticle concentration and (b) temperature with various values of regular Lewis number of salt 2 'Le_2'. There is no direct coupling between the nanoparticle concentration equation (14) and either of the salt diffusion equations (12, 13). However all three species equations are coupled to the momentum equation (10) via the respective species buoyancy terms, $\lambda[\theta + Nc_1\chi_1 + Nc_2\chi_2 - Nr\phi]$. $Le_2 = \dfrac{\upsilon}{D_{S_2}}$ and represents the relative momentum diffusion rate to the species (salt 2) molecular diffusion rate. There is therefore an interaction between the velocity field and all three species diffusion fields. Increment in Le_2 clearly significantly enhances the nanoparticle concentration values throughout the boundary layer implying that a reduction in salt 2 diffusivity encourages the migration of nanoparticles away from the wall into the boundary layer. This will efectively reduce mass transfer of nanoparticles to the wall. Closer to the wall linear stretching boosts the

nanoparticle concentration (Fig 17a) whereas further from the wall, in the post-peak zone, nonlinear stretching amplifes nanoparticle concentration. Temperature is also noticeably hiked with a reise in in Le_2 and this pattern is consistent throughout the boundary layer regime. Linear stretching produces higher temperatures in close proximity to the wall; however very quickly this behaviour is modified and thereafter sustained. Thermal boundary layer thickness is therefore boosted with higher salt 2 regular Lewis number owing to the enormous decrease in salt 2 molecular diffusivity.

Figure 18 presents the influence of nanofluid Lewis number 'Ln' on dimensionless nanoparticle concentration. This parameter is distinct from the salt solutal Lewis numbers. $Ln = \frac{\upsilon}{D_B}$ relates the momentum diffusion rate to the nanoparticle molecular diffusivity. It arises only in the nanoparticle concentration equation (14), in the term, $+\left(\frac{n+1}{2}\right) Lnf\phi'$ which produces an interplay between the momentum and nanoparticle diffusion fields. As *Ln* is increased there is a considerable depletion in nanoparticle mass diffusivity. This counteracts the migration of nanoparticles into the boundary layer and strongly depletes nanoparticle concentration (volume fraction). Nanoparticle boundary layer thickness is therefore also decreased signfiicantly. With linear stretching (n = 1), again there is an initial elevation in nanoparticle concentrations near the wall; however further from the wall, non-linear (n = 0.5) stretching achieves markedly higher values of nanoparticle concentration.

Figure 19 visualizes the impact of magnetic field parameter 'Mn' on solutal concentrations of (a) salt 1, (b) salt 2. The magnetohydrodynamic body force appears in the momentum equation (10) as Lorentzian drag force, $-Mn(f')$. Although this term is linear, the effect of Mn is profound. $Mn = \frac{\sigma B_o^2}{\left(\rho_{f\infty}\right)\alpha}$ and expresses the relative contribution of magnetic force to inertial force in the regime. It is a modified form of the Stuart magnetic interaction number. When *Mn* = 1 both forces contribute equally. In Fig 19a, b several values of *Mn* are considered. When *Mn* = 0 magnetic force vanishes and the nanopolymer is *electrically non-conducting*. *Mn* > 1 implies dominance of the magnetic (Lorentz) force to the inertial force. Both salt 1 concentration χ_1 and salt 2 concentration χ_2 are boosted significantly with increment in Mn. The damping of the boundary layer flow (deceleration) reduces the momentum diffusion rate. Via coupling of the salt 1 and 2 species conservation equations (12, 13) with the momentum equation (11), both χ_1 and χ_2 are affected. The retardation in the flow exacerbates salt species

mass diffusion and increases sat 1 and 2 species boundary layer thicknesses. Clearly thinner species boundary layers are produced for *Mn* = 0. The implication is that a non-intrusive magnetic field can be successfully exploited to manipulate the salt diffusion characteristics in nanopolymers. Both salt 1 and 2 concentration magnitudes exhibit a smooth montonic decay from the wall and higher magnitudes always correspond to the nonlinear stretching scenario (*n* = 0.5).

Figure 20 presents the evolution in ffect of (a) nanoparticle concentration and (b) temperature with alteration in the magnetic field parameter '*Mn*'. Although *Mn* is absent in both the nanoparticle and thermal boundary layer equations (11) and (14), these equations, as noted earlier exhibit strong coupling to the momentum equation (10). The presence of a magnetic field therefore indirectly influences both nanoparticle diffusion and thermal energy distribution in the boundary layer. Nanoparticle concentrations are greatly reduced whereas temperature is strongly enhanced with stronger magnetic parameter values. Nanoparticle diffusion is inhibited by transverse magnetic field [28] and responds differently to salt species concentrations (which due the ionic nature is enhanced). The supplementary work expended in dragging the nanpolymer against the action of the transverse magnetic field is dissipated as heat. This energizes the boundary layer and elevates temperatures. Thermal boundary layer thickness is therefore boosted. Additonally, nonlinear stretching inhibits nanoparticle concentration (thinner nanoparticle species boundary layer) whereas it enhances temperatures (thicker thermal boundary layer). Overall the combined action of stretching and magnetic field intensity are very potent techniques for manipulating the transport (and distribution) of nanoparticles and cooling effect in nanopolymer fabrication.

Figure 21 depicts the impact of (a) magnetic field parameter 'Mn' on dimensionless velocity and (b) Brownian motion parameter 'Nb' on nanoparticle concentration. As elaborated earlier the Lorentzian drag force is accentuated with increment in *Mn*. This will substantially damp the boundary layer flow and elevate hydrodynamic boundary layer thickness (Fig. 21a). Effective flow control of the stretching sheet coating regime is therefore attainable via modification in the external magnetic field. The magnetohydrodynamic technique is inexpensive and is therefore popular in materials processing [14]. The effect of random, chaotic motion of nanoparticles in the regime is simulated with the Brownian motion parameter, *Nb*. This features in the Buongiorno nanoscale term, $+\frac{Nt}{Nb}\theta''$ in equation (14) and also in the modified wall boundary condition, $Nb\phi'(0) + Nt\theta'(0) = 0$ in equation (15).

Larger values of *Nb* imply smaller nanoparticle diameters and vice versa. As *Nb* increases the nanoparticle concentration (Fig. 21b) is reduced since ballistic collisions and macroscopic convection around the nanoparticles is reduced. The nanoparticle concentration boundary layer thickness is therefore also decreased. Both velocity and nanoparticle concentration are maximum with nonlinear sheet stretching (n = 0.5).

Figure 22: shows the influence of modified Dufour parameter of salt 1 'Nd_1' on solutal concentrations of (a) salt 1 and (b) salt 2. $Nd_1 = \dfrac{\sigma D_{TC_1}\left(C_{1w} - C_{1\infty}\right)}{\alpha\left(T_f - T_\infty\right)}$ and occurs in the term, $+Nd_1\chi_1''$ in the energy equation (11). An increase from negative to positive values of this parameter substantially reduces both the salt 1 concentration χ_1 and salt 2 concentration χ_2 magnitudes. Negative values of 'Nd_1' imply that species buoyancy and thermal buoyancy are opposing whereas positive values imply they are assistive. Clearly the former case increases the species boundary layer thicknesses for both salts whereas the latter reduces them. Slightly greater magnitudes of both salt concentrations are obtained for the nonlinear stretching sheet case (n = 0.5) compared with the linear stretching case (n = 1).

Figure 23 illustrate the effect of modified Dufour parameter of salt 1 'Nd_1' on dimensionless (a) nanoparticle concentration and (b) temperature. Nanoparticle concentration is generally decerased with increment in Nd_1 whereas temperature are noticeably elevated. A strong heating effect is therefore generated in the regime whereas nanoparticle diffusion is stifled. Thermal boundary layer thickness will therefore be accentuated whereas nanoparticle boundary layer thickness will be reduced.

Figure 24 shows the influence of modified Dufour parameter of salt 2 'Nd_2' on solutal concentrations of (a) salt 1 and (b) salt 2. $Nd_2 = \dfrac{\sigma D_{TC_2}\left(C_{2w} - C_{2\infty}\right)}{\alpha\left(T_f - T_\infty\right)}$ and features also in the energy equation (11) via the term, $+Nd_2\chi_2''$. A boost in this parameter implies a stronger diffuso-thermal (Dufour) effect associated with salt 2. This results in a significant suppression in both salt concentrations i.e. reduction in magnitudes of χ_1 and χ_2. Both salt solute boundary layer thicknesses will therefore also be reduced. Both profiles are also increasingly parabolic for positive values of Nd_2 whereas a linear decay is computed with negative values of Nd_2. Nonlinear stretching again generates greater magnitudes in both salt concentration profiles comapred with linear stretching.

Figure 25: displays the distributions for (a) nanoparticle concentration and (b) temperature with a change in modified Dufour parameter of salt 2 'Nd_2'. Initially there is an increase in nanoparticle concentration with positive Nd_2 values close to the wall; this is however reversed further from the wall where negative values of the modified Dufour parameter of salt 2 achieve greater magnitudes. Temperature is however consistently enhanced with negative values of Nd_2 and reduced with positive values. The temperature is also greater for the nonlinear stretching case and therefore thermal boundary layers will be thicker.

Figure 26 presents the effect of thermophoresis parameter 'Nt' on dimensionless nanoaprticle concentration. Thermophoresis referes to the migration of nanoparticles under a strong temperature gradient to a colder zone. As *Nt* is increased, after a short distance into the boundary layer, nanoparticle concentrations are observed to be elevated significantly with stronger thermophoresis effect. However closer to the wall linear stretching is associated with higher magnitudes (thicker nanoparticle boundary layer thickness) whereas further from the wall greater magnitudes corrrespond to nonlinear stretching.

5.Conclusions

A theoretical study has been presented, motivated by smart nanopolymer flow processing, for the *steady two-dimensional magnetohydrodynamic triple diffusive free convection of nanofluid from a vertical stretching sheet in a porous medium*. Separate concentration equations are featured for dual diffusing salts (species 1 and 2) in addition to nanoparticle mass transfer. The Buongiorno two-component nanoscale framework is deployed which also features Brownian motion and thermophoretic body force effects. Soret (thermo-diffusion) and Dufour (diffuso-thermo) effects for both salt species are incorporated. Following non-dimensionalization and transformation of the governing boundary layer equations and associated wall and free stream conditions, the resulting 11^{th} order nonlinear ordinary differential boundary value problem is solved numerically with MATLAB's bvp4c code. The effects of the emerging parameters velocity, temperature and concentration distributions are plotted and discussed. The present simulations have shown that:

- The simulatenous deployment of nanoparticles and dual salt species stongly modifies temperature distributions and will therefore influence wall heat transfer rates.

- An increase in magnetic parameter damps the velocity, reduces nanoparticle concentration, increases temperature and also boosts both salt species 1 and 2 concentrations.
- An increase in the modified Dufour parameter of salt 1 increases temperature and salt 1 and salt 2 concentrations (and the associated boundary layer thicknesses) but reduces the nanoparticle concentration magnitudes.
- A rise in modified Dufour parameter of salt 2 suppresses nanoparticle concentration further from the wall and also generally reduces the salt 1 and salt 2 concentrations. However temperature is boosted with negative values of modified Dufour parameter of salt 2 but reduced with positive values.
- Nanoparticle concentration and boundary layer thickness are both reduced with an increment in Brownian motion parameter.
- The concentrations of both salts are found to be higher for larger Lewis numbers.
- Nonlinear stretching generally increases velocity, temperature and species concentrations for the nanoparticles and salts, whereas linear stretching induces the opposite effect.
- The effect of increasing the thermal buoyancy parameter is to reduce both the thermal and concentration boundary-layer thicknesses.
- The dimensionless velocity increases with increasing species buoyancy ratio of each salt in *assisting* flows and with decreasing buoyancy ratio in *opposing* flows.

The present study has revealed some interesting characteristics of nonlinear triple diffusive convection in magneto-nanofluid stretching boundary layer flows. Attention has however been restricted to Newtonian behaviour. Future investigations may consider a range of non-Newtonian effects including viscoplasticity, viscoelasticity and microstructural behaviour and will be communcated imminently.

References

[1] S.U.S. Choi, Enhancing thermal conductivity of fluids with nanoparticles, in: *D.A. Siginer, H.P. Wang (Eds.), Developments and Applications of Non-Newtonian Flows, ASME FED*, vol. 231, 1995, pp. 99-105.

[2] Y. Ding, H. Chen, L. Wang, C.-Y Yang, Y. Hel, W. Yang, W.P. Lee, L. Zhang, R. Huo, Heat transfer intensification using nanofluids, *Kona* 25 (2007) 23-38.

[3] S.U.S. Choi, Z.G. Zhang, W. Yu, F.E. Lockwood, E.A. Grulke, Anomalously thermal conductivity enhancement in nanotube suspensions, *Appl. Phys. Lett.* 79 (2001) 2252-2254.

[4] R. Ellahi, A. Zeeshan, F. Hussain and T. Abbas, Study of shiny film coating on multi-fluid flows of a rotating disk suspended with nano-sized silver and gold particles: a comparative analysis, *Coatings*, 2018, 8, 422; doi:10.3390/coatings8120422.

[5] Smaisim, G.F., *et al.*, Nanofluids: properties and applications. *Journal of Sol-Gel Science and Technology*, 2022: p. 1-35.

[6] Mukherjee, S., et al., A review on pool and flow boiling enhancement using nanofluids: *Nuclear reactor application. Processes*, 2022. 10(1): p. 177.

[7] Pordanjani, A.H., *et al.*, An updated review on application of nanofluids in heat exchangers for saving energy. *Energy Conversion and Management*, 2019. 198: p. 111886.

[8] S. Chinchanikar *et al*., A review on nanofluids in minimum quantity lubrication machining, *Journal of Manufacturing Processes*, 68, 2021, 56-70.

[9] Islam MR, Shabani B, Rosengarten G. Nanofluids to improve the performance of PEM fuel cell cooling systems: a theoretical approach. *Appl Energy*. 2016; 178:660–71.

[10] Gherasim O, Ficai A, Andronescu E. Biomedical applications of silver nanoparticles: an up-to-date overview. *Nanomaterials.* 2018; 8:1–25.

[11] Jayati Tripathi, B. Vasu and O. Anwar Bég, Computational simulations of hybrid mediated nano- hemodynamics (Ag-Au/blood) through an irregular symmetric stenosis, *Computers in Biology and Medicine 130 (2021).* 104213 doi.org/10.1016/j.compbiomed.2021.104213

[12] Sireetorn Kuharat, O. Anwar Bég, B. Vasu, Ali Kadir, Tasveer A. Bég, H.J. Leonard, W.S. Jouri and J.C. Umavathi, Numerical study of buoyancy-driven convection in a trapezoidal solar enclosure with zinc and diamond nanoparticles, *Book chapter, Green Energy and Energy Storage", CRC, Taylor and Francis, USA (2022).*

[13] K. Thirumalaisamy, R. Sivaraj, V. R. Prasad, O. Anwar Bég, H-H. Leung, F. Kamalov and K. Vajravelu, Comparative heat transfer analysis of γAl2O3 and γ-Al2O3-C2H6O2 electroconductive nanofluids in a saturated porous square cavity with Joule dissipation and heat source/sink effects, *Physics of Fluids, 34, 072001 (2022); (21 pages)* https://doi.org/10.1063/5.0095334

[14] Y. Jaluria, Heat and mass transfer in the extrusion of non-Newtonian materials. *Adv. Heat Tran.* 28, 145–230 (1996).

[15] J. Buongiorno, Convective transport in nanofluids, *ASME J. Heat Transfer* 128 (2006) 240-250.

[16] W. A. Khan, A. Aziz, Double-diffusive Natural Convective boundary layer flow in a porous medium saturated with a nanofluid over a vertical surface: Prescribed surface heat, solute and nanoparticle fluxes, *Int. J. Therm. Sci*. 50 (2011) 2154-2160.

[17] A.V. Kuznetsov, D.A. Nield, Double-diffusive natural convective boundary layer flow of a nanofluid past a vertical plate, *Int. J. Therm. Sci.* 50 (2011) 712-717.

[18] W. A. Khan, I. Pop, Boundary-layer flow of a nanofluid past a stretching sheet, *Int. J. Heat Mass Transfer*. 53 (2010) 2477-2483.

[19] Atul Kumar Ray, B. Vasu, P. V. S. N. Murthy, O. Anwar Bég, R.S.R. Gorla and B. Kumar, Convective flow of non-homogeneous rheological nanofluids with non-Fourier thermal relaxation -application in polymer coating, *Arabian J. Science Engineering (2021).* https://doi.org/10.1007/ s13369-021-06467-w (18 pages).

[20] A. K. Ray, B Vasu, O. Anwar Bég, R. S R Gorla and P. V. S. N. Murthy, Homotopy semi-numerical modelling of non-Newtonian nanofluid transport external to multiple geometries using a revised Buongiorno model, *Inventions, 4, 54, 1-27 (2019). doi:10.3390/inventions 4040054 (2019).*

[21] B. Vasu, R.S.R. Gorla, P. V. S. N. Murthy and O. Anwar Bég, Entropy analysis on convective film flow of power-law fluid with nanoparticles along an inclined plate, *J. Applied Mechanics and Technical Physics, 60, 5, 1-15 (2019).*

[22] I.Nkurikiyimfura *et al.*, Heat transfer enhancement by magnetic nanofluids—A review *Renewable and Sustainable Energy Reviews,* 21, 2013, 548-561.

[23] S. Akar *et al.*, Targeting a channel coating by using magnetic field and magnetic nanofluids, *Journal of Thermal Analysis and Calorimetry*, 137, 381–388 (2019).

[24] M. Ali Abbas, O. Anwar Bég, A. Zeeshan, A. Hobiny, M. M. Bhatti, Parametric analysis and minimization of entropy generation in bioinspired magnetized non-Newtonian nanofluid pumping using artificial neural networks and particle swarm optimization, *Thermal Science and Engineering Progress* (2021). doi.org/10.1016/j.tsep.2021.100930 (10 pages)

[25] S.O. Solawu, M. Shamshuddin, O. Anwar Bég, Influence of magnetization, variable viscosity and thermal conductivity on Von Karman swirling flow of H_2O-Fe_3O_4 and H_2O-Mn-$ZNFe_2O_4$ ferromagnetic nanofluids from a stretchable rotating disk: smart spin coating simulation, *Materials Science and Engineering B (USA). 279 (2022) 115659 (13 pages).*

[26] Kim HSS, Sohn BHH, Lee W *et al.*, Multifunctional layer-by-layer self-assembly of conducting polymers and magnetic nanoparticles. *Thin Solid Films* 419:173–177, 2002.

[27] Poddar P, Wilson JL, Srikanth H *et al.* Magnetic properties of conducting polymer doped with manganese–zinc ferrite nanoparticles. *Nanotechnology* 15: S570–S574, 2004.

[28] Xiao HM, Zhang WD, Wan MX, Fu SY, Novel electromagnetic functionalized γ-Fe_2O_3/polypyrrole composite nanostructures with high conductivity. *J Polym Sci, Part A: Polym Chem* 47:4446–4453, 2009.

[29] M.I. Anwar *et al.*, Computational analysis of induced magnetohydrodynamic non-Newtonian nanofluid flow over nonlinear stretching sheet, 2022, *Progress in Reaction Kinetics and Mechanism*, Volume 47, 2022. doi.org/10.1177/14686783211072712

[30] Hussain T, Shehzad SA, Hayat T, *et al.* Radiative hydromagnetic flow of Jeffrey nanofluid by an exponentially stretching sheet. *Plos One* 2014; 9(8): e103719.

[31] Bég OA, Khan MS, Karim I, *et al.* Explicit numerical study of unsteady hydromagnetic mixed convective nanofluid flow from an exponentially stretching sheet in porous media. *Appl Nanosci* 2014; 4(8): 943–957.

[32] Y. Jaluria, Heat and mass transfer in materials processing and manufacturing, *Advances in Heat Transfer*, 48, 2016, Pages 1-94.

[33] T. Hayat and F.A. Hendi, Thermal-diffusion and diffusion thermo effects on MHD three-dimensional axisymmetric flow with Hall and ion-slip currents, *Journal of American Science*, vol. 8, pp. 284-294, 2012.

[34] A.A. Afify, Similarity solution in MHD: effects of thermal diffusion and diffusion thermo on free convective heat and mass transfer over a stretching surface considering suction or injection, *Comm. Nonlinear Science Numerical Simulation*, vol. 14, no. 5, pp. 2202-2214, 2009.

[35] D. Pal and H. Mondal, MHD non-Darcy mixed convective diffusion of species over a stretching sheet embedded in a porous medium with non-uniform heat source/sink, variable viscosity and Soret effect, *Comm. Nonlinear Science Numerical Simulation*, vol. 17, no. 2, pp. 672-684, 2012.

[36] O. A. Bég, V. R. Prasad, B. Vasu, N. B. Redd, Q. Li, and R. Bhargava, Free Convection heat and mass transfer from an isothermal sphere to a micropolar regime with Soret/Dufour effects, *International Journal Heat Mass Transfer*, vol. 54, no. 1-3, pp. 9-18, 2011.

[37] Dzulkifli NF, Bachok N, Pop I, Yacob NA, Arifin NM, Rosali H (2017) Soret and Dufour effects on unsteady boundary layer flow and heat transfer of nanofluid over a stretching/shrinking sheet: a stability analysis. *J Chem Eng Process Technol.,* 8:1000336.

[38] J.C. Umavathi and O. Anwar Bég, Computation of thermo-solutal convection with Soret-Dufour cross diffusion in a vertical duct containing carbon/metallic nanofluids, *Proc. IMeche Part C- J. Mechanical Engineering, UK (2022). DOI: 10.1177/09544062211072693 (17 pages*

[39] M.I. Anwar *et al.*, Soret–Dufour and radiative aspects in hydromagnetized nanofluid flow in stratified porous medium, *SN Applied Sciences*, volume 1, Article number: 1430 (2019)

[40] M.M. Bhatti, C.M. Khalique, Tasveer Bég, O. Anwar Bég and Ali Kadir, Numerical study of slip and radiative effects on magnetic Fe_3O_4-water-based nanofluid flow from a nonlinear stretching sheet in porous media with Soret and Dufour diffusion, *Modern Physics Letters B 33*, 2050026 (24 pages) (2020).

[41] S. Rionero, Triple diffusive convection in a porous medium, *Acta Mech*. 224(2013) 447-458.

[42] J.C. Umavathi and O. Anwar Bég, Mathematical modelling of triple diffusion in natural convection flow in a vertical duct with Robin boundary conditions, viscous heating and chemical reaction effects, *J. Engineering Thermophysics,* 29 (2) 1–26 (2020).

[43] Z.H. Khan *et al.,* Triple convective-diffusion boundary layer along a vertical flat plate in a porous medium saturated by a water-based nanofluid, *International Journal of Thermal Sciences*, 90, 2015, 53-61.

[44] Long YY-Z, Chen Z, Duvail JL *et al.* (2005) Micro- and nano-structured conducting polymeric materials. *Prog Polym Sci.*, 35:1673.

[45] MD. Shamshuddin, S.R. Mishra, O. Anwar Bég, T.A. Bég and Ali Kadir, Computation of radiative Marangoni (thermocapillary) magnetohydrodynamic convection in Cu-water based nanofluid flow from a disk in porous media: smart coating simulation, *Heat Transfer (2020). DOI: 10.1002/htj.21963 (20 pages)*

[46] J.C. Umavathi and O. Anwar Bég, Simulation of the onset of convection in porous medium layer saturated by a couple stress nanofluid, *Microfluidics and Nanofluidics (2021). 25:53 https://doi.org/10.1007/s10404-021-02448-5 (20 pages).*

[47] J.C. Umavathi and O. Anwar Bég, Double diffusive convection in a dissipative electrically conducting nanofluid under orthogonal electrical and magnetic field: *a numerical study, Nanoscience and Technology: An International Journal, 12 (2), 59-90 (2021).*